

Endo-exo framework for a unifying classification of episodic landslide movements

Qinghua Lei¹ and Didier Sornette²

¹Uppsala University

²SUSTech

February 16, 2024

Abstract

We propose the “endo-exo” conceptual framework to account for the varied and complex episodic landslide movements observed during progressive maturation until collapse/stabilization. This framework captures the interplay between exogenous stressors such as rainfall and endogenous damage/healing processes. The underlying physical picture involves cascades of local triggered mass movements due to fracturing and sliding. We predict four distinct types of episodic landslide dynamics (exogenous/endogenous-subcritical/critical), characterized by power-law relaxations with different exponents, all related to a single parameter β . These predictions are tested on the dataset of the Preonzo landslide, which exhibited multi-year episodic movements prior to a final collapse. All episodic activities can be accounted for within this classification with $|\beta - 0.45| \leq 0.1$, providing strong support for our parsimonious theory. We further show that the final catastrophic failure of this landslide is clearly preceded by an increased frequency of large velocities corresponding to a transition to a supercritical regime with amplifying positive feedbacks.

Hosted file

Manuscript.docx available at <https://authorea.com/users/744415/articles/717409-endo-exo-framework-for-a-unifying-classification-of-episodic-landslide-movements>

1 **Endo-exo framework for a unifying classification of episodic landslide movements**

2
3 **Qinghua Lei¹, Didier Sornette²**

4 ¹Department of Earth Sciences, Uppsala University, Uppsala, Sweden

5 ²Institute of Risk Analysis, Prediction and Management, Academy for Advanced
6 Interdisciplinary Studies, Southern University of Science and Technology, Shenzhen, China

7 Correspondence: Qinghua Lei (qinghua.lei@geo.uu.se)

8 **Key Points:**

- 9 • A novel endo-exo framework is established to classify episodic landslide dynamics into
10 four types and validated on a real landslide
- 11 • The theory is very parsimonious with a single adjusted parameter accounting for all four
12 power-law regimes of episodic landslide movements
- 13 • The transition of the landslide from episodic to catastrophic movements is clearly
14 preceded by an increased frequency of large velocities

15 Abstract

16 We propose the “endo-exo” conceptual framework to account for the varied and complex
17 episodic landslide movements observed during progressive maturation until collapse/stabilization.
18 This framework captures the interplay between exogenous stressors such as rainfall and
19 endogenous damage/healing processes. The underlying physical picture involves cascades of
20 local triggered mass movements due to fracturing and sliding. We predict four distinct types of
21 episodic landslide dynamics (exogenous/endogenous-subcritical/critical), characterized by
22 power-law relaxations with different exponents, all related to a single parameter ϑ . These
23 predictions are tested on the dataset of the Preonzo landslide, which exhibited multi-year
24 episodic movements prior to a final collapse. All episodic activities can be accounted for within
25 this classification with $\vartheta \approx 0.45 \pm 0.1$, providing strong support for our parsimonious theory.
26 We further show that the final catastrophic failure of this landslide is clearly preceded by an
27 increased frequency of large velocities corresponding to a transition to a supercritical regime
28 with amplifying positive feedbacks.

29 Plain Language Summary

30 Landslides involve complex gravity-driven downslope movements developing over days
31 to years before a possible major collapse, which are commonly boosted and/or driven by external
32 events like precipitations and earthquakes. The reasons behind these episodic movements,
33 characterized by alternating cycles of accelerating-decelerating creeps (marked by intermittent
34 bursts of displacement followed by sustained periods of relaxation dynamics) and how they
35 relate to the final instability remain poorly understood. Here, we propose a new “endo-exo”
36 theory to classify episodic landslide movements into four fundamental types, based on the
37 precursory/recovery properties of their associated intermittent velocity peaks. We provide a
38 thorough demonstration of our theory based on the long-term monitoring dataset of a rainfall-
39 induced landslide at Preonzo, Switzerland, which episodically moved over many years and
40 eventually collapsed catastrophically in 2012. We observe all four types of episodic dynamics in
41 the Preonzo landslide with their precursory/recovery properties consistent with our theoretical
42 prediction. We further propose a new metric, obtainable from slope displacement monitoring
43 data, as a precursor to catastrophic landslides. Our novel conceptual framework points at the
44 existence of a deep quantitative relationship between episodic landslide movements, external
45 triggering events (e.g., rainfall, snowmelt, and seismicity), and internal slip, damage, and healing
46 processes within the landmass.

47 1. Introduction

48 Landslides, a widespread form of mass wasting, occur in various Earth surface
 49 environments and pose significant threats to life and property worldwide (Palmer, 2017). Due to
 50 rapid population growth and urbanization, human habitats are increasingly exposed to landslide
 51 hazards, with the situation becoming even more severe under climate change, where extreme
 52 rainfall, permafrost thaw, and glacier retreat have promoted fatal landslides (Gariano & Guzzetti,
 53 2016; Lacroix et al., 2022; Patton et al., 2021). Extensive field observations show that landslides
 54 commonly exhibit episodic movements characterized by intermittent acceleration-deceleration
 55 sequences that are boosted by external events like precipitations and earthquakes (Agliardi et al.,
 56 2020; Bontemps et al., 2020; Cappa et al., 2014; Crosta et al., 2014, 2017; Finnegan et al., 2022;
 57 Handwerger et al., 2013; Lacroix et al., 2014). Some landslides have episodically crept over
 58 hundreds or thousands of years, while others could evolve into a major collapse after
 59 episodically deforming over days to years (Lacroix et al., 2020). The reasons behind these
 60 episodic movements (marked by intermittent bursts of displacement followed by sustained
 61 periods of relaxation dynamics) and how they relate to a possible final catastrophic failure
 62 remain poorly understood, inhibiting our capability to predict landslide behavior and mitigate the
 63 associated risks.

64 We identify the following fundamental questions: (a) Are episodic landslide movements
 65 of an exogenous or endogenous origin? (b) What are their underlying mechanisms? (c) How do
 66 they relate to catastrophic failures? In this Letter, we propose to answer these questions by
 67 establishing a novel “endo-exo” framework to quantitatively classify landslide episodic
 68 movements as well as decipher their exogenous/endogenous origins and triggering mechanisms.
 69 The rest of the Letter is organized as follows. Section 2 elaborates the mathematical foundation
 70 of this endo-exo framework. Section 3 presents a demonstration of how our theory applies, based
 71 on a real landslide dataset. Finally, a discussion on the above fundamental questions is given in
 72 Section 4.

73 2. Theory

74 We conceptualize a landslide as a complex system consisting of numerous geomaterial
 75 masses interacting via cohesive or frictional contacts. The displacement activity of the landslide
 76 results from a combination of external forces like precipitations and earthquakes, and of internal
 77 influences where each past moved mass may prompt other masses in its network of interactions
 78 to move as a result of the redistribution of mechanical stress, pore pressure, and possibly other
 79 physico-chemical fields. This impact of a mass on other masses is not instantaneous, due to the
 80 time-dependent nature of the relevant geomechanical processes like creep, damage, and friction
 81 (Scholz, 2019). This latency can be described by a memory kernel $\psi(t - \tau)$, giving the
 82 probability that the movement of a mass at time τ leads to the movement at a later time t by
 83 another mass in direct interaction with the first moved mass. This memory kernel $\psi(t - \tau)$ can
 84 be seen as a fundamental macroscopic description of how long it takes for a mass to be triggered
 85 to move following the interaction with an already moved neighbouring mass. In other words, it is
 86 a “bare” propagator, describing the distribution of waiting times between “cause” and “action”
 87 for a mass to move, which may obey a power-law characterizing a long-memory process
 88 (Saichev & Sornette, 2010b; Sornette, 2006b; Sornette & Helmstetter, 2003):

$$89 \quad \psi(t - \tau) \propto 1/(t - \tau)^{1+\vartheta}, \text{ with } 0 < \vartheta < 1 \text{ and for } t - \tau > c \quad (1)$$

90 where the exponent $\vartheta > 0$ controls the persistence of memory and c is a small characteristic time
 91 scale regularizing the singularity at $t - \tau = 0$. For instance, one way to implement the
 92 regularization is to replace $1/(t - \tau)^{1+\vartheta}$ by $1/(t - \tau + c)^{1+\vartheta}$. Such a regularization is essential
 93 to make the integral of $\psi(t)$ finite and thus ensure a valid theory. Physically, this ensures the
 94 finiteness of the number of mass movements triggered by a preceding one. The assumption that
 95 $\psi(t)$ has a power-law tail is supported by many empirical observations such as Andrade’s law of
 96 material creep and Omori’s law of aftershock activity (see Helmstetter & Sornette, 2002; Nechad
 97 et al., 2005a, 2005b; Saichev & Sornette, 2005; Sornette & Sornette, 1999; and references
 98 therein).

99 Starting from an initial moved mass, i.e., the “mother” mass, which first displaces due to
 100 either external forces or internal fluctuations, it may trigger the movements of first-generation
 101 “daughter” masses nearby, which themselves trigger their own daughter masses to move, and so
 102 on. Such an epidemic process can be captured by a conditional self-excited point process
 103 (Hawkes & Oakes, 1974), which can be mapped exactly onto a branching process, such that the
 104 average of the displacement rate (i.e., velocity) of the mass system is governed by the following
 105 self-consistent equation (Sornette, 2006b; Sornette & Helmstetter, 2003):

$$106 \quad v(t) = V(t) + n \int_{-\infty}^t \psi(t - \tau) v(\tau) d\tau, \quad (2)$$

107 where $V(t)$ is the exogenous source that is not triggered by any epidemic effect in the system
 108 and $n \geq 0$ is the effective branching ratio defined as the average number of moving daughter
 109 masses triggered by a mother mass that moved in the past. Expression (2) is the equation for the
 110 first-order moment (or average) of the velocity, whose underlying dynamics is given by a self-
 111 excited point process. The branching ratio n depends on the network topology of geomaterial
 112 masses and the spreading behavior of disturbances in the system, therefore reflecting the
 113 maturation of the landslide, with $n < 1$, $n \simeq 1$, and $n > 1$ corresponding to the subcritical,
 114 critical, and supercritical regimes, respectively (Harris, 1963; Sornette, 2006a). Here, we mainly
 115 focus on the subcritical and critical regimes with $n \lesssim 1$ to ensure stationarity, whereas the
 116 transition into the supercritical regime $n > 1$ related to the emergence of a catastrophic failure
 117 (Helmstetter & Sornette, 2002; Sornette & Helmstetter, 2002) will be discussed in section 4.

118 Considering the exogenous source $V(t)$ given by a delta function $\delta(t)$ centered at the
 119 origin of time, we obtain the Green function of equation (2), also called a dressed or
 120 renormalized memory kernel $\Psi(t - \tau)$, which is the solution of (Helmstetter & Sornette, 2002;
 121 Sornette & Helmstetter, 2003)

$$122 \quad \Psi(t) = \delta(t) + n \int_{-\infty}^t \psi(t - \tau) \Psi(\tau) d\tau, \quad (3)$$

123 such that

$$124 \quad v(t) = \int_{-\infty}^t V(\tau) \Psi(t - \tau) d\tau, \quad (4)$$

125 which is the solution of equation (2). Equation (4) expresses the fact that the present velocity
 126 $v(t)$ results from all past exogenous sources $V(\tau)$ mediated to the present by the dressed
 127 memory kernel $\Psi(t - \tau)$ incorporating all the generations of cascades of influences (Sornette,
 128 2006b). For the case where the bare propagator is given by equation (1), the recovery dynamics
 129 of the system after a strong external event $V(\tau) \propto \delta(\tau - t_c)$ is fully controlled by the dressed
 130 memory kernel (Sornette & Helmstetter, 2003), such that:

$$131 \quad v(t) = \Psi(t) \propto \begin{cases} 1/(t - t_c)^{1-\vartheta}, & \text{for } c < t - t_c < t^*, \\ 1/(t - t_c)^{1+\vartheta}, & \text{for } t - t_c > t^*, \end{cases} \quad (5)$$

132 where t_c is the critical time chosen as the time of the peak and t^* is the characteristic time given
133 by (Helmstetter & Sornette, 2002):

$$134 \quad t^* = c \left(\frac{n\Gamma(1-\vartheta)}{|1-n|} \right)^{1/\vartheta} \propto |1-n|^{-1/\vartheta}. \quad (6)$$

135 Thus, it can be seen that, as $n \rightarrow 1$ (critical regime), $t^* \rightarrow +\infty$, so that the short-term response
136 prevails ($t - t_c < t^*$); as $n \rightarrow 0$ (pure noncritical regime), $t^* \rightarrow c$ and the long-term response
137 dominates ($t - t_c > t^*$); if $0 < n < 1$ (subcritical regime), t^* has a finite value and the system
138 may manifest a coexistence of both short- and long-term responses.

139 In the absence of strong external events, a peak in landslide velocity can also
140 spontaneously occur due to the interplay of a continuous stochastic flow of small external
141 perturbations and the amplifying impact of the epidemic cascade of endogenous interactions. The
142 average velocity trajectory before and after the peak, conditioned on the existence of a peak, is
143 given by $\langle v(t) | v(t_c) \rangle \propto \text{Cov}(v(t), v(t_c))$, so the precursory and recovery dynamics associated
144 with the peak are governed by (Helmstetter et al., 2003; Sornette & Helmstetter, 2003):

$$145 \quad v(t) \propto \int_{-\infty}^{t-t_c} \Psi(t - t_c - \tau) \Psi(-\tau) d\tau \propto 1/|t - t_c|^{1-2\vartheta}, \text{ for } c < |t - t_c| < t^*, \quad (7)$$

146 or equivalently for $n \rightarrow 1$ (critical regime). If $n < 1$ (subcritical regime), the system response is
147 essentially a noise process largely driven by random fluctuations (Crane & Sornette, 2008):

$$148 \quad v(t) \propto 1/|t - t_c|^0, \text{ for } |t - t_c| > t^*. \quad (8)$$

149 From the above derivations, we can see that landslide velocities around a peak at time t_c
150 can be described by a generalized power-law as:

$$151 \quad v(t) \propto 1/|t - t_c|^p, \quad (9)$$

152 where the exponent p depends on the parameter ϑ and the regime. This allows us to classify
153 episodic landslide movements into four fundamental types based on a combination of the origin
154 of disturbance (exogenous/endogenous) and the cascading behavior (subcritical/critical) (Crane
155 & Sornette, 2008):

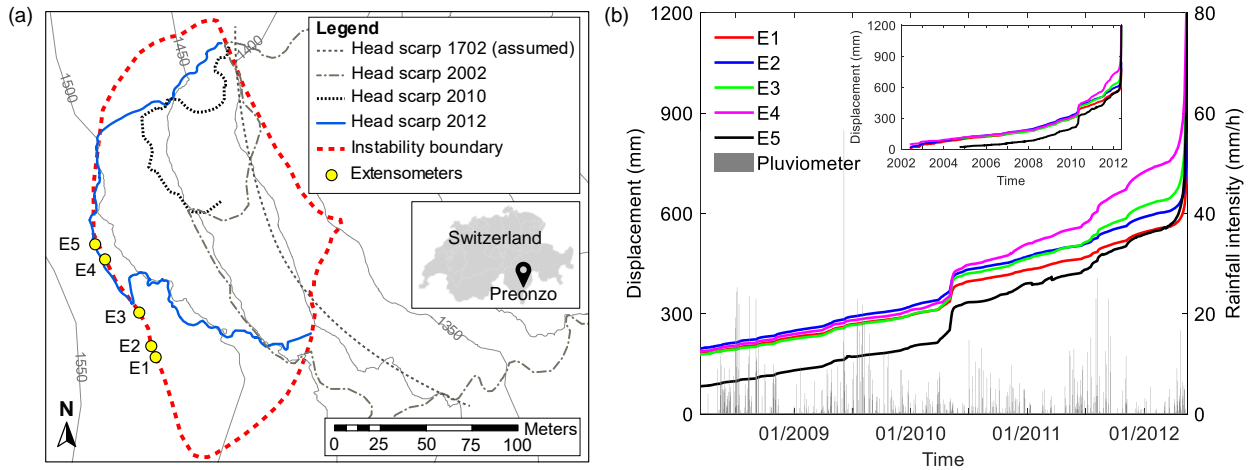
- 156 • Type I: Exogenous-subcritical, with $p = 1 + \vartheta$ for $t - t_c > t^*$. Here, the system is not
157 “ripe” and the cascading propensity is limited ($n < 1$), meaning that the exogenously
158 induced displacement activity at time t_c does not cascade beyond the first few
159 generations of triggered masses. The post-peak velocity relaxation is thus governed by
160 the bare memory kernel.
- 161 • Type II: Exogenous-critical, with $p = 1 - \vartheta$ for $c < t - t_c < t^*$. Here, the system is
162 ripe ($n \simeq 1$), such that the exogenously induced displacement activity at time t_c
163 cascades through the system of interconnected masses, triggering neighbouring masses
164 that further trigger their own neighbouring masses and so on. The post-peak velocity
165 relaxation is governed by the dressed memory kernel.
- 166 • Type III: Endogenous-subcritical, with $p = 0$ for $|t - t_c| > t^*$. The displacement
167 activity does not result from an exogenous event but instead from an endogenous

168 forcing. The system is not ripe ($n < 1$) such that no cascade develops and the (small)
 169 peak is associated with no apparent precursory/recovery signatures.

- 170 • Type IV: Endogenous-critical, with $p = 1 - 2\vartheta$ for $c < |t - t_c| < t^*$. The
 171 displacement activity originates from endogenous growth/interaction within the ripe
 172 system ($n \simeq 1$), where the triggering cascades produce an approximately symmetrical
 173 power-law acceleration-deceleration behaviour around the peak.

174 This classification arises from the interplay of the bare long-memory process as embodied in
 175 equation (1) and the epidemic cascade throughout the system as captured by equation (2). It can
 176 be seen that the relaxation following an endogenous-critical peak (with a smaller exponent
 177 $p = 1 - 2\vartheta$) is slower than that following an exogenous-critical peak (with a larger exponent
 178 $p = 1 - \vartheta$). This longer-lived influence of an endogenous-critical peak results from the
 179 precursory process that impregnates the system much more than its exogenous counterpart
 180 (Sornette et al., 2004).

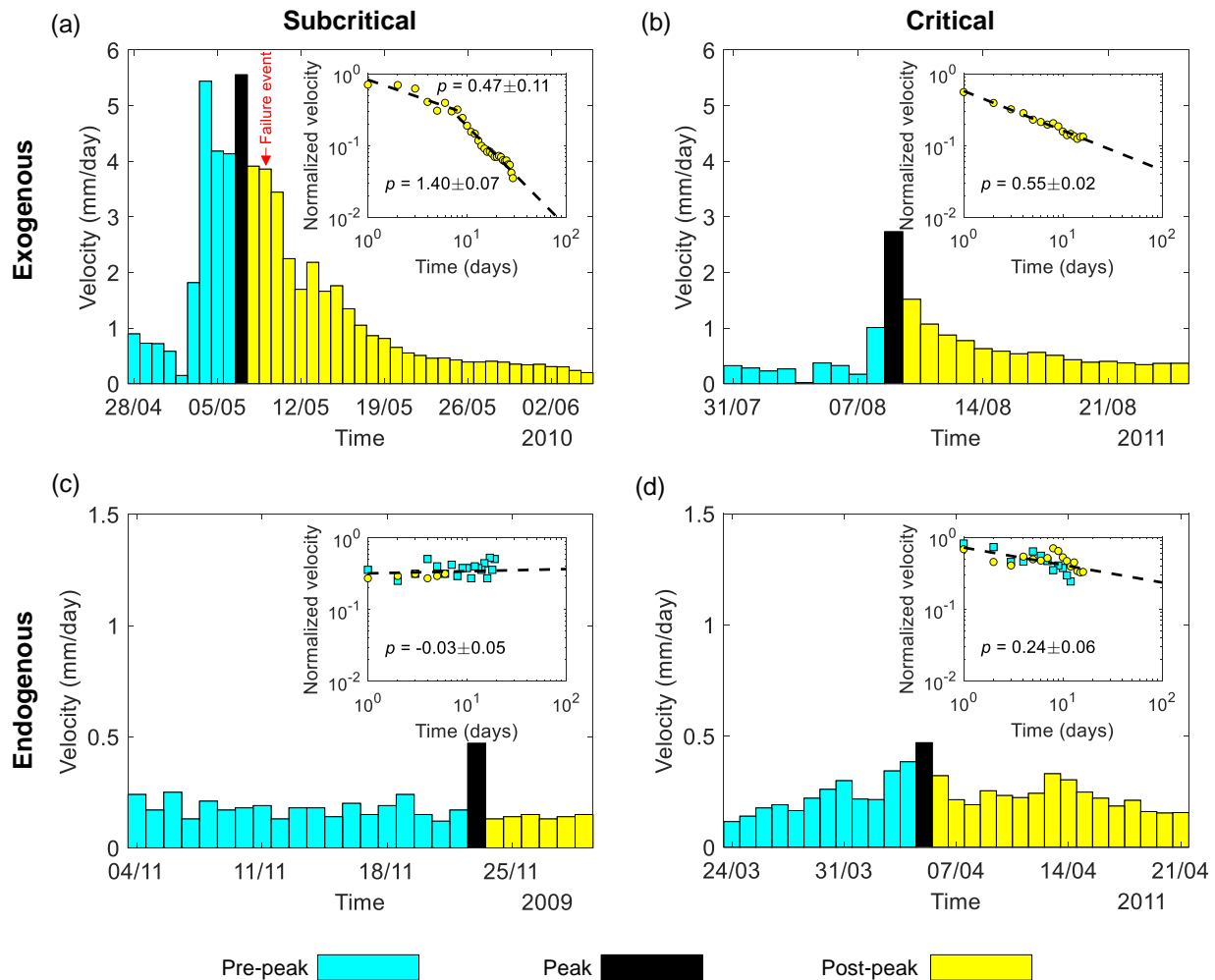
181 3. Dataset and Analysis



182
 183 **Figure 1.** (a) Overview of the Preonzo landslide, Switzerland with the locations of five
 184 extensometers E1-E5, the boundary of this instability complex, and the headscarps of historical
 185 failure events indicated. (b) Monitoring data of slope displacements by the five extensometers
 186 and recorded data of rainfall intensity by a pluviometer installed at the slope.

187 We test our theory based on the long-term monitoring dataset of a rainfall-induced
 188 landslide at Preonzo, Switzerland, which exhibited significant episodic movements over many
 189 years prior to a catastrophic failure in 2012 (Lei et al., 2023; Lei & Sornette, 2023; Loew et al.,
 190 2017). This active landslide has experienced multiple failures since the 18th century (Gschwind
 191 et al., 2019) (see the head scarps of historical events in Figure 1a). To closely monitor this
 192 instability complex that posed a great threat to the industrial and transport infrastructures located
 193 directly at the toe of the slope, five high-precision extensometers E1-E5 (see Figure 1a for their
 194 locations) were instrumented to measure the opening of tension cracks in the headscarp area.
 195 From 2008, a pluviometer was installed to monitor the local precipitation conditions. Figure 1b
 196 shows the time series of slope displacement measured by the five extensometers and of rainfall
 197 intensity recorded by the pluviometer between 2008 and 2012 (see the inset for the displacement
 198 time series from 2002 and Figure S1 in the Supporting Information for the time series of

199 daily/cumulative rainfall amounts). One can see that this landslide exhibited a step-like
 200 deformation pattern over time as it progressively destabilized, leading up to a catastrophic failure
 201 on 15 May 2012. The displacement curve consists of numerous creep episodes (i.e., repeated
 202 cycles of accelerating-decelerating creeps) that often show a good coincidence with the
 203 occurrence of intense rainfall events.



204

205 **Figure 2.** Four categories of episodic landslide dynamics found in the velocity time series of the
 206 Preonzo landslide: (a) Type I, exogenous-subcritical; (b) Type II, exogenous-critical; (c) Type III,
 207 endogenous-subcritical; and (d) Type IV, endogenous-critical. The red arrow in (a) marks the
 208 timing of the local failure of a downslope northern sector of the slope on 9 May 2010. Insets
 209 show the post-peak relaxation of normalized velocity where dashed lines indicate the power-law
 210 fitting.

211 We compute slope velocities on a daily basis from the displacement time series recorded
 212 by the five extensometers. All the four types of episodic landslide dynamics, viz.,
 213 exogenous/endogenous-subcritical/critical, can be found in the velocity time series (see Figures 2
 214 and 3 for typical examples). We fit the data of normalized velocities to a power-law (see Text S1
 215 and S2 in the Supporting Information for the normalized velocity calculation and fitting
 216 algorithm).

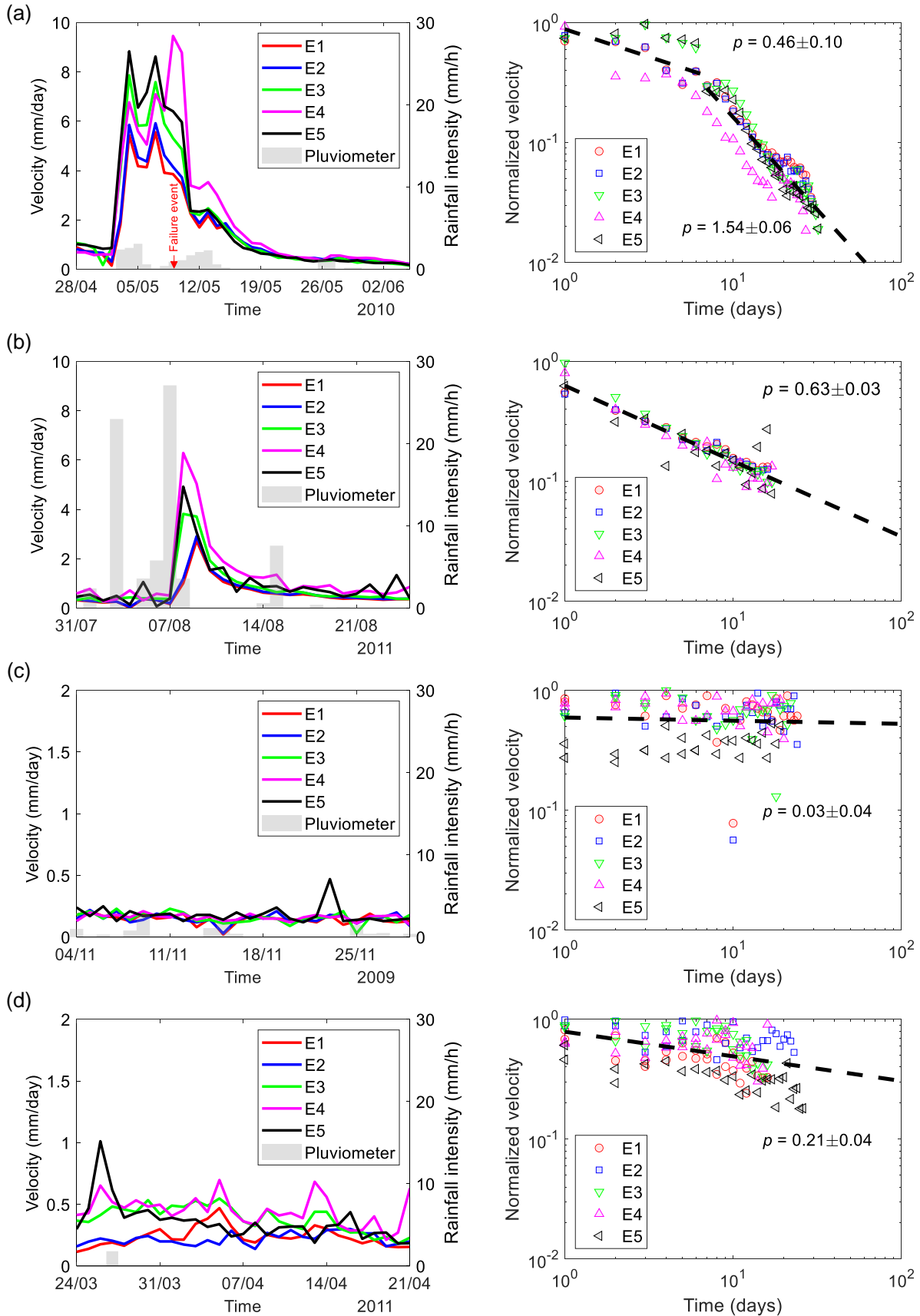
217 For the Type I peak on 7 May 2010 (Figure 2a), the velocity relaxation beyond ~8 days
218 after the peak is characterized by an exponent of $p = 1.40 \pm 0.07$ (exogenous-subcritical)
219 (Figure 2a, inset), whereas its short-term response within ~8 days after the peak is associated
220 with a much smaller exponent of $p = 0.47 \pm 0.11$ (exogenous-critical), as expected from the
221 prediction by equation (5). All five extensometers exhibit a similar two-branch power-law
222 relaxation behavior with an exponent of $p = 0.46 \pm 0.10$ for the short-term response and an
223 exponent of $p = 1.54 \pm 0.06$ for the long-term response (Figure 3a; see also Figure S2 in the
224 Supporting Information for the power-law fitting for individual extensometers). Around this peak
225 accompanied by mild precipitation (Figure 3a, left), the slope has experienced a localized failure
226 in its northern sector downhill from the tension cracks where the extensometers are installed (see
227 Figure 1a for the head scarp and section 4 for a discussion of the possible triggering
228 mechanisms).

229 For the Type II peak on 9 August 2011 (Figure 2b), the post-peak velocity relaxation
230 obeys a power-law with an exponent of $p = 0.55 \pm 0.02$ (exogenous-critical) (Figure 2b, inset).
231 Prior to this peak, a heavy rainstorm has occurred (Figure 3b, left). All the five extensometers
232 have captured this peak followed by a power-law relaxation with an overall exponent of $p =$
233 0.63 ± 0.03 (Figure 3b; see also Figure S3 in the Supporting Information for the power-law
234 fitting for individual extensometers).

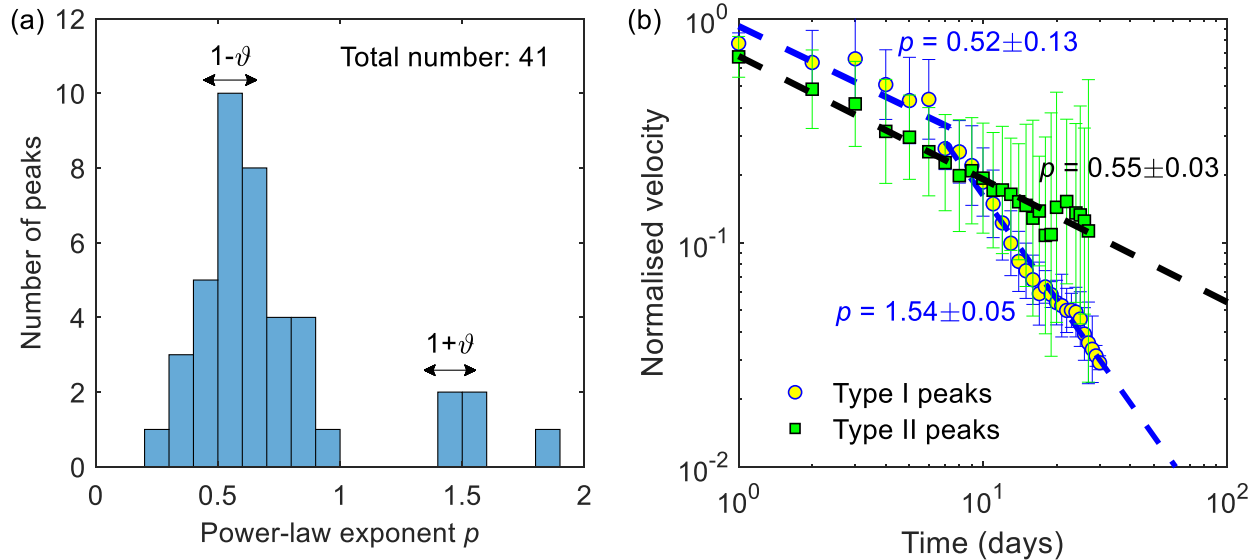
235 In Figure 2c, we present a Type III endogenous-subcritical peak preceded by no rainfall
236 event (Figure 3c). This peak is surrounded by an essentially time-independent velocity trajectory
237 with $p \approx 0$ (Figure 3c), whereas most extensometers do not capture this peak and only show
238 random fluctuations (Figure 3c and Figure S4 in the Supporting Information).

239 Lastly, we show a Type IV endogenous-critical peak (Figure 2d), which occurs after a
240 progressively accelerating power-law growth of velocity followed by an approximately
241 symmetrical power-law relaxation, with a common exponent of $p = 0.24 \pm 0.06$. It seems that
242 the majority of the five extensometers has captured such an approximately symmetrical
243 precursory-recovery dynamics with a small power-law exponent of $p = 0.21 \pm 0.04$ (Figure 3d),
244 although the timing of the peaks recorded by individual extensometers is not fully synchronized
245 (Figure S5 in the Supporting Information). One can notice that the time-dependent signatures of
246 endogenous peaks are less apparent compared to exogenous ones (as reflected by the notable
247 dispersion of the data in Figures 2d and 3d).

248 Interpreting these results in light of equations (5), (7) and (8), the obtained power-laws
249 for these different peak types point to the existence of a single parameter $\vartheta \approx 0.45 \pm 0.10$,
250 providing strong support for our theory.



252 **Figure 3.** Slope velocity time series measured by the five extensometers E1-E5 as well as
 253 rainfall intensity data recorded by the pluviometer (left panel) and post-peak velocity relaxation
 254 (right panel) for different types of peaks: (a) Type I, exogenous-subcritical; (b) Type II,
 255 exogenous-critical; (c) Type III, endogenous-subcritical; and (d) Type IV, endogenous-critical.
 256 The red arrow in (a) marks the timing of the local failure of a northern sector of the slope on 9
 257 May 2010. In (c) and (d) right, pre-peak velocity data are also indicated (open markers) in
 258 addition to post-peak data (filled markers).



259 **Figure 4.** (a) Histogram of power-law exponents p for post-peak velocity relaxation. The double
 260 arrows indicate the value ranges of $p = 1 - \vartheta$ (Type I peaks) and $p = 1 + \vartheta$ (Type II peaks),
 261 with $\vartheta \approx 0.45 \pm 0.1$. (b) Ensemble averaged velocity relaxation behavior for Type I and II
 262 peaks; error bars indicate the standard deviation associated with the ensemble average.
 263

264 We implement a peak detection algorithm to automatically extract slope velocity peaks
 265 together with their surrounding time series from the 10-year long-term monitoring dataset. We
 266 qualify a peak in the velocity time series as a local maximum over a 20-day time window which
 267 is at least $k = 2.5$ times larger than the average velocity over a 2-month time window. The time
 268 window sizes and threshold value k are chosen to give an effective detection of good-quality
 269 peaks (see Figure S2 in the Supporting Information), but the results do not significantly change
 270 by varying these parameters (see Figures S7-S10 and S13-S14 in the Supporting Information). In
 271 addition, we request that each peak has at least 10 days of post-peak data before reaching the
 272 next peak. In total, our algorithm detects 104 peaks from the entire dataset recorded by five
 273 extensometers. We then fit the post-peak velocity data of each detected peak to a power-law (see
 274 Text S2 in the Supporting Informaiton) over a time window ranging from 10 to 30 days, with the
 275 “best” window chosen as the one giving the highest coefficient of determination R^2 . We only
 276 keep the peaks with $R^2 > 0.8$ to extract unambiguous post-peak response functions, leaving 41
 277 peaks. In Figure 4a, we show the histogram of their power-law exponents p , which cluster into
 278 two distinct groups, one with a median at $p \approx 0.59$ and the other with a median at $p \approx 1.52$.
 279 This result is compatible with our theoretical prediction based on $\vartheta \approx 0.45 \pm 0.10$, yielding
 280 $p \approx 1.45 \pm 0.10$ for Type I peaks and $p \approx 0.55 \pm 0.10$ for Type II peaks. It seems that Type III
 281 and IV peaks (with $p \approx 0$ or 0.1 ± 0.20) are absent in Figure 4a. This is because they usually

282 have small magnitudes and considerably fluctuating post-peak responses (Figure 2c-d and Figure
 283 3c-d), making it difficult for them to pass the criteria of $k = 2.5$ and $R^2 > 0.8$. We then compute
 284 the ensemble average of the relaxation behavior for the two exogenous peak types (Figure 4b),
 285 with the fitted power-laws consistent with the existence of a single parameter $\vartheta \approx 0.45 \pm 0.10$.
 286 Our results in Figure 4 do not qualitatively change by varying the k threshold from 1.5 to 3.5 and
 287 the R^2 threshold from 0.7 to 0.9 as well as the window sizes for peak detection (Figures S12-S14
 288 in the Supporting Information), suggesting that our method and results are robust.

289 4. Discussion

290 We have presented a novel endo-exo theoretical framework to quantitatively classify
 291 episodic landslide movements into four fundamental types of distinct precursory/recovery
 292 signatures but related by a single common parameter ϑ . All the four types of landslide dynamics
 293 have been observed in the Preonzo landslide with $\vartheta \approx 0.45 \pm 0.10$, which is different from the
 294 mean-field solution $\vartheta \approx 0$ for creep ruptures in heterogeneous materials (Nechad et al., 2005a,
 295 2005b; Saichev & Sornette, 2005). Such a non-mean-field response reflects the intrinsic
 296 fluctuations and correlations resulting from triggered cascades of geomaterial mass motions in
 297 the landslide. This ϑ value close to 0.5 may be explained by the first-passage problem of an
 298 underlying random walk (Redner, 2001; Saichev & Sornette, 2010a), where a daughter mass
 299 surrounding a mobilized mother mass is only triggered to move when the fluctuating stress first
 300 reaches the strength level for sliding or fracturing.

301 Our results reveal that many rainfall-induced velocity peaks of the Preonzo landslide
 302 belong to the exogenous-critical type, meaning that the landslide dynamics in response to
 303 external perturbations is dominated by cascades involving high-order generations of mass
 304 movement triggering and the collective response of the entire mass population is slower and
 305 more persistent (governed by the dressed memory kernel with an exponent of $1 - \vartheta$) than the
 306 individual mass response (governed by the bare memory kernel with an exponent of $1 + \vartheta$). This
 307 implies that this landslide is operating around a critical state with the branching ratio n
 308 intermittently increasing and receding close to 1, likely due to the competing damage and healing
 309 processes. This physical picture refines the concept of self-organized criticality stating that many
 310 crustal phenomena like earthquakes and landslides are evolving in a statistically stationary state
 311 of marginal stability (Bak & Tang, 1989; Hergarten & Neugebauer, 1998; Main, 1996; Sornette
 312 & Sornette, 1989; Sornette, 2006a; Turcotte, 1999). Such a paradigm explains why some rainfall
 313 events could trigger episodic landslide movements while others do not (Figure 3), which is
 314 simply due to the dynamically evolving nature of the system that is relaxed away (but not far)
 315 from the critical state after each peak and then attracted back to the the critical state over time
 316 mediated by a continuous flow of external perturbations (e.g., rainfall, snowmelt, and diurnal
 317 temperature/humidity cycles). In addition, we have documented a unique exogenous-subcritical
 318 type of episodic landslide dynamics, which is related to the local failure of a downslope sector of
 319 the slope on 9 May 2010 (Loew et al., 2017). Before showing a rapid exogenous-subcritical
 320 relaxation characterized by a large exponent of $1 + \vartheta$, the landslide has actually experienced ~ 8
 321 days of relatively slower exogenous-critical relaxation with a small exponent of $1 - \vartheta$ (see
 322 Figures 2a and 3a). Substituting this characteristic time $t^* \approx 8$ days together with $\vartheta \approx 0.45$ into
 323 equation (6) and the estimate $c \approx 1$ day, we obtain $n \approx 0.63$. This comparatively low n value is
 324 consistent with the fact that this local failure-induced shock did not lead to a system-sized
 325 collapse since only a few generations of failure cascades have developed. Contrarily, the high n

326 value for rainfall-induced exogenous-critical shocks may be due to the fact that the disturbance
 327 by rainwater infiltration is likely to affect the entire slope and thus has a stronger spreading
 328 behavior. In our dataset, we also observe the presence of endogenous-critical landslide dynamics,
 329 indicating that cascading mass movements play a dominant role in triggering landslides through
 330 a kind of self-organized criticality. However, they are usually associated with small-magnitude
 331 peaks and weak time-dependence (governed by a relaxation exponent of $1 - 2\vartheta$ close to 0),
 332 making them sometimes difficult to be discriminated from the endogenous-subcritical dynamics
 333 driven by random fluctuations.

334 Up to now, we have mainly focused on the “endo-exo” regime where the landslide
 335 evolution is characterized by numerous accelerating-decelerating creep episodes driven by the
 336 interplay of exogenous perturbation and endogenous maturation. As the mass of the landslide
 337 progressively weakens, it could transition into the supercritical regime with $n > 1$ (Harris, 1963;
 338 Sornette, 2006a), where the number of triggering events in the system grows on average
 339 exponentially with time (Helmstetter & Sornette, 2002) or even faster (Sornette & Helmstetter,
 340 2002). This critical transition is found to be often endogenously driven in different natural and
 341 social systems (Sornette, 2006b), which explains why many rainfall-induced landslides
 342 catastrophically fail in the absence of exceptional precipitation events (Eberhardt, 2008). If the
 343 supercritical regime is dominated by positive feedbacks with the slope acceleration behavior
 344 $\dot{v}(t) \propto v(t)^m$ characterized by $m > 1$, the system would exhibit a finite-time singularity and
 345 thus a catastrophic failure (Lei et al., 2023; Lei & Sornette, 2023; Sornette, 2002).

346 We fit the velocity time series of the Preonzo landslide prior to its catastrophic failure on
 347 15 May 2012 to a power-law in the form of equation (9) with $p = 1/(m - 1)$, yielding a two-
 348 branch behavior with $p \approx 1.88$ ($m \approx 1.53$) for the early stage and $p \approx 0.49$ ($m \approx 3.04$) for the
 349 late stage (Figure S15 in the Supporting Information). This suggests that the system is indeed
 350 dominated by positive feedbacks which seem to become even stronger close to the final collapse.
 351 Our previous work showed that those late stage large velocities are “dragon-kings” (Lei et al.,
 352 2023) — a double metaphor for an event of a predominant impact/size like a “king” and a unique
 353 origin like a “dragon” (Sornette & Ouillon, 2012). This break in power-law scaling thus marks
 354 the transition of the system from the self-organised criticality regime where a catastrophic failure
 355 is unpredictable (the so-called “black-swan” regime) (Taleb, 2010) to the dragon-king regime
 356 where a catastrophic failure is predictable (Sornette & Ouillon, 2012). Interestingly, when
 357 entering the dragon-king regime, the system once experienced a temporary deceleration during
 358 7-11 May 2012 just before the final collapse and such a precursory quiescence is consistent with
 359 the theoretical prediction for the supercritical regime with $n > 1$ and $\vartheta > 0$ (Helmstetter &
 360 Sornette, 2002). Substituting $t^* \approx 4$ days and $\vartheta \approx 0.45$ into equation (6) which also holds for the
 361 supercritical regime (Helmstetter & Sornette, 2002), we obtain $n \approx 7.46$, indicating an intense
 362 explosive branching process. Considering the analogue between landslides and earthquakes
 363 (Finnegan et al., 2022; Gomberg et al., 1995; Handwerker et al., 2016; Helmstetter et al., 2004;
 364 Lacroix et al., 2014), we postulate that the condition for this subcritical/critical-to-supercritical
 365 transition to occur is that the system shifts from $\alpha < \mu$ to $\alpha \geq \mu$ (Sornette & Helmstetter, 2002),
 366 where α is the exponent in the productivity law $\rho(E) \propto E^\alpha$ defining the number of daughter
 367 masses triggered by a mother mass of energy release E and μ is the exponent in the Gutenberg-
 368 Richter-type density distribution of daily energy release of the landslide $f(E(t)) \propto E(t)^{-(1+\mu)}$.
 369 Given $E(t) \propto v(t)^2$, we derive $f(v(t)) \propto v(t)^{-(1+2\mu)}$ from the law of conservation of
 370 probability under a change of variable (Sornette, 2006a). Our previous work suggests that the

371 probability distribution of the $v(t)$'s of the Preonzo landslide follow an inverse gamma
 372 distribution (with β denoting its shape parameter) characterized by a power-law tail $f(v(t)) \propto$
 373 $v(t)^{-(1+\beta)}$ (Lei & Sornette, 2023), with therefore $\beta = 2\mu$. It is found that β progressively drops
 374 from 1.92 to 1.76 (correspondingly, μ drops from 0.96 to 0.88) over ~ 1 month time (Figure S16
 375 in the Supporting Information), suggesting an increased frequency of large velocities as the slope
 376 approaches the critical transition from the endo-exo regime (dominated by small velocities) to
 377 the dragon-king regime (dominated by large velocities) occurring at ~ 1 week before the final
 378 collapse (Lei et al., 2023). Thus, we would expect $\alpha \approx 0.88$, which is comparable to the typical
 379 value of $\alpha \approx 0.8$ for earthquakes (Helmstetter, 2003). This correspondence holds
 380 notwithstanding the fact that landslides happen in near-surface environments under low stress
 381 conditions, while earthquakes occur in deep subsurface regions subject to much higher stress
 382 levels. The decrease of β prior to catastrophic landslides is similar to the observed b -value
 383 decline prior to great earthquakes (Imoto, 1991; Nakaya, 2006; Smith, 1981), which is possibly
 384 due to increased differential stresses on rock bridges/asperities accommodating crack
 385 propagations (Scholz, 2015) and/or enhanced differential stresses on creeping fault patches
 386 promoting slip ruptures (Ito & Kaneko, 2023). It has also a natural interpretation within the
 387 physical picture of cascades of triggered events as described by self-excited conditional point
 388 processes (Helmstetter & Sornette, 2003). This observation points to the possibility to predict
 389 catastrophic landslides by monitoring the temporal evolution of the β -value.

390 Our novel conceptual framework points at the existence of a deep quantitative
 391 relationship between episodic landslide movements, external triggering events (e.g., rainfall,
 392 snowmelt, and seismicity), and internal frictional slip, damage, and healing processes within the
 393 landmass. Based on the well-documented dataset of the Preonzo landslide, we have provided a
 394 thorough validation of this framework, which can be further applied to many other landslides
 395 showing similar episodic movements (Agliardi et al., 2020; Bontemps et al., 2020; Cappa et al.,
 396 2014; Crosta et al., 2014, 2017; Finnegan et al., 2022; Handwerker et al., 2013; Lacroix et al.,
 397 2014). The results and insights obtained in this Letter have important implications for landslide
 398 hazard prediction and mitigation.

399 **Acknowledgement**

400 Q.L. is grateful for the support by the Swiss National Science Foundation (Grant No.
 401 189882) and the National Natural Science Foundation of China (Grant No. 41961134032). D.S.
 402 acknowledges partial support from the National Natural Science Foundation of China (Grant No.
 403 U2039202), from the Shenzhen Science and Technology Innovation Commission (Grant No.
 404 GJHZ20210705141805017) and the Center for Computational Science and Engineering at
 405 Southern University of Science and Technology.

406 **Open Research**

407 The slope displacement monitoring data of the Preonzo landslide are publicly available at
 408 the ETH Zurich Research Collection (<https://doi.org/10.3929/ethz-b-000600495>).

409 **References**

410 Agliardi, F., Scuderi, M. M., Fusi, N., & Collettini, C. (2020). Slow-to-fast transition of giant
 411 creeping rockslides modulated by undrained loading in basal shear zones. *Nature*
 412 *Communications*, *11*(1), 1–11. <https://doi.org/10.1038/s41467-020-15093-3>

- 413 Bak, P., & Tang, C. (1989). Earthquakes as a self-organized critical phenomenon. *Journal of*
414 *Geophysical Research: Solid Earth*, 94(B11), 15635–15637.
415 <https://doi.org/10.1029/JB094iB11p15635>
- 416 Bontemps, N., Lacroix, P., Larose, E., Jara, J., & Taïpe, E. (2020). Rain and small earthquakes
417 maintain a slow-moving landslide in a persistent critical state. *Nature Communications*,
418 11(1), 1–10. <https://doi.org/10.1038/s41467-020-14445-3>
- 419 Cappa, F., Guglielmi, Y., Viseur, S., & Garambois, S. (2014). Deep fluids can facilitate rupture
420 of slow-moving giant landslides as a result of stress transfer and frictional weakening.
421 *Geophysical Research Letters*, 41(1), 61–66. <https://doi.org/10.1002/2013GL058566>
- 422 Crane, R., & Sornette, D. (2008). Robust dynamic classes revealed by measuring the response
423 function of a social system. *Proceedings of the National Academy of Sciences of the United*
424 *States of America*, 105(41), 15649–15653. <https://doi.org/10.1073/pnas.0803685105>
- 425 Crosta, G. B., di Prisco, C., Frattini, P., Frigerio, G., Castellanza, R., & Agliardi, F. (2014).
426 Chasing a complete understanding of the triggering mechanisms of a large rapidly evolving
427 rockslide. *Landslides*, 11(5), 747–764. <https://doi.org/10.1007/s10346-013-0433-1>
- 428 Crosta, G. B., Agliardi, F., Rivolta, C., Alberti, S., & Dei Cas, L. (2017). Long-term evolution
429 and early warning strategies for complex rockslides by real-time monitoring. *Landslides*,
430 14(5), 1615–1632. <https://doi.org/10.1007/s10346-017-0817-8>
- 431 Eberhardt, E. (2008). Twenty-ninth Canadian Geotechnical Colloquium: The role of advanced
432 numerical methods and geotechnical field measurements in understanding complex deep-
433 seated rock slope failure mechanisms. *Canadian Geotechnical Journal*, 45(4), 484–510.
434 <https://doi.org/10.1139/T07-116>
- 435 Finnegan, N. J., Brodsky, E. E., Savage, H. M., Nereson, A. L., & Murphy, C. R. (2022).
436 Seasonal slow landslide displacement is accommodated by mm-scale stick-slip events.
437 *Geophysical Research Letters*, 49(20), e2022GL099548.
438 <https://doi.org/10.1029/2022GL099548>
- 439 Gariano, S. L., & Guzzetti, F. (2016). Landslides in a changing climate. *Earth-Science Reviews*,
440 162, 227–252. <https://doi.org/10.1016/j.earscirev.2016.08.011>
- 441 Gomberg, J., Bodin, P., Savage, W., & Jackson, M. E. (1995). Landslide faults and tectonic
442 faults, analogs?: The Slumgullion earthflow, Colorado. *Geology*, 23(1), 41–44.
443 [https://doi.org/10.1130/0091-7613\(1995\)023<0041:LFATFA>2.3.CO;2](https://doi.org/10.1130/0091-7613(1995)023<0041:LFATFA>2.3.CO;2)
- 444 Gschwind, S., Loew, S., & Wolter, A. (2019). Multi-stage structural and kinematic analysis of a
445 retrogressive rock slope instability complex (Preonzo, Switzerland). *Engineering Geology*,
446 252, 27–42. <https://doi.org/10.1016/j.enggeo.2019.02.018>
- 447 Handwerger, A. L., Roering, J. J., & Schmidt, D. A. (2013). Controls on the seasonal
448 deformation of slow-moving landslides. *Earth and Planetary Science Letters*, 377–378,
449 239–247. <https://doi.org/10.1016/j.epsl.2013.06.047>
- 450 Handwerger, A. L., Rempel, A. W., Skarbak, R. M., Roering, J. J., & Hilley, G. E. (2016). Rate-
451 weakening friction characterizes both slow sliding and catastrophic failure of landslides.
452 *Proceedings of the National Academy of Sciences of the United States of America*, 113(37),
453 10281–10286. <https://doi.org/10.1073/pnas.1607009113>
- 454 Harris, T. E. (1963). *The Theory of Branching Processes*. Berlin: Springer.
- 455 Hawkes, A. G., & Oakes, D. (1974). A cluster process representation of a self-exciting process.
456 *Journal of Applied Probability*, 11(3), 493–503. <https://doi.org/10.2307/3212693>
- 457 Helmstetter, A. (2003). Is earthquake triggering driven by small earthquakes? *Physical Review*
458 *Letters*, 91(5), 3–6. <https://doi.org/10.1103/PhysRevLett.91.058501>

- 459 Helmstetter, A., & Sornette, D. (2002). Subcritical and supercritical regimes in epidemic models
 460 of earthquake aftershocks. *Journal of Geophysical Research: Solid Earth*, *107*(B10), ESE
 461 10-1-ESE 10-21. <https://doi.org/10.1029/2001JB001580>
- 462 Helmstetter, A., & Sornette, D. (2003). Predictability in the Epidemic-Type Aftershock
 463 Sequence model of interacting triggered seismicity. *Journal of Geophysical Research: Solid
 464 Earth*, *108*(B10), 2482. <https://doi.org/10.1029/2003JB002485>
- 465 Helmstetter, A., Sornette, D., & Grasso, J.-R. (2003). Mainshocks are aftershocks of conditional
 466 foreshocks: How do foreshock statistical properties emerge from aftershock laws. *Journal
 467 of Geophysical Research: Solid Earth*, *108*(B1), 1–24.
 468 <https://doi.org/10.1029/2002JB001991>
- 469 Helmstetter, A., Sornette, D., Grasso, J.-R., Andersen, J. V., Gluzman, S., & Pisarenko, V.
 470 (2004). Slider block friction model for landslides: Application to Vaiont and La Clapière
 471 landslides. *Journal of Geophysical Research: Solid Earth*, *109*(B2), 1–15.
 472 <https://doi.org/10.1029/2002jb002160>
- 473 Hergarten, S., & Neugebauer, H. J. (1998). Self-organized criticality in a landslide model.
 474 *Geophysical Research Letters*, *25*(6), 801–804. <https://doi.org/10.1029/98GL50419>
- 475 Imoto, M. (1991). Changes in the magnitude-frequency b-value prior to large ($M \geq 6.0$)
 476 earthquakes in Japan. *Tectonophysics*, *193*(4), 311–325. [https://doi.org/10.1016/0040-1951\(91\)90340-X](https://doi.org/10.1016/0040-1951(91)90340-X)
- 477
 478 Ito, R., & Kaneko, Y. (2023). Physical mechanism for a temporal decrease of the Gutenberg-
 479 Richter b -value prior to a large earthquake. *Journal of Geophysical Research: Solid Earth*,
 480 *128*(12), 1–21. <https://doi.org/10.1029/2023JB027413>
- 481 Lacroix, P., Perfettini, H., Taïpe, E., & Guillier, B. (2014). Coseismic and postseismic motion of
 482 a landslide: Observations, modeling, and analogy with tectonic faults. *Geophysical
 483 Research Letters*, *41*(19), 6676–6680. <https://doi.org/10.1002/2014GL061170>
- 484 Lacroix, P., Handwerker, A. L., & Bièvre, G. (2020). Life and death of slow-moving landslides.
 485 *Nature Reviews Earth & Environment*, *1*(8), 404–419. <https://doi.org/10.1038/s43017-020-0072-8>
- 486
 487 Lacroix, P., Belart, J. M. C., Berthier, E., Sæmundsson, P., & Jónsdóttir, K. (2022). Mechanisms
 488 of landslide destabilization induced by glacier-retreat on Tungnakvíslarjökull area, Iceland.
 489 *Geophysical Research Letters*, *49*(14), 1–11. <https://doi.org/10.1029/2022GL098302>
- 490 Lei, Q., & Sornette, D. (2023). A stochastic dynamical model of slope creep and failure.
 491 *Geophysical Research Letters*, *50*(11), e2022GL102587.
 492 <https://doi.org/10.1029/2022GL102587>
- 493 Lei, Q., Sornette, D., Yang, H., & Loew, S. (2023). Real-time forecast of catastrophic landslides
 494 via dragon-king detection. *Geophysical Research Letters*, *50*(6), e2022GL100832.
 495 <https://doi.org/10.1029/2022GL100832>
- 496 Loew, S., Gschwind, S., Gischig, V., Keller-Signer, A., & Valenti, G. (2017). Monitoring and
 497 early warning of the 2012 Preonzo catastrophic rock slope failure. *Landslides*, *14*(1), 141–
 498 154. <https://doi.org/10.1007/s10346-016-0701-y>
- 499 Main, I. (1996). Statistical physics, seismogenesis, and seismic hazard. *Reviews of Geophysics*,
 500 *34*(4), 433–462. <https://doi.org/10.1029/96RG02808>
- 501 Nakaya, S. (2006). Spatiotemporal variation in b value within the subducting slab prior to the
 502 2003 Tokachi-oki earthquake ($M 8.0$), Japan. *Journal of Geophysical Research: Solid
 503 Earth*, *111*(B3), 1–13. <https://doi.org/10.1029/2005JB003658>
- 504 Nechad, H., Helmstetter, A., El Guerjouma, R., & Sornette, D. (2005a). Andrade and critical

- 505 time-to-failure laws in fiber-matrix composites: Experiments and model. *Journal of the*
 506 *Mechanics and Physics of Solids*, 53(5), 1099–1127.
 507 <https://doi.org/10.1016/j.jmps.2004.12.001>
- 508 Nechad, H., Helmstetter, A., El Guerjouma, R., & Sornette, D. (2005b). Creep ruptures in
 509 heterogeneous materials. *Physical Review Letters*, 94(4), 045501.
 510 <https://doi.org/10.1103/PhysRevLett.94.045501>
- 511 Palmer, J. (2017). Creeping earth could hold secret to deadly landslides. *Nature*, 548(7668),
 512 384–386. <https://doi.org/10.1038/548384a>
- 513 Patton, A. I., Rathburn, S. L., Capps, D. M., McGrath, D., & Brown, R. A. (2021). Ongoing
 514 landslide deformation in thawing permafrost. *Geophysical Research Letters*, 48(16), 1–11.
 515 <https://doi.org/10.1029/2021GL092959>
- 516 Redner, S. (2001). *A Guide to First-Passage Processes*. Cambridge: Cambridge University
 517 Press. <https://doi.org/10.1017/CBO9780511606014>
- 518 Saichev, A., & Sornette, D. (2005). Andrade, Omori, and time-to-failure laws from thermal noise
 519 in material rupture. *Physical Review E*, 71(1), 016608.
 520 <https://doi.org/10.1103/PhysRevE.71.016608>
- 521 Saichev, A., & Sornette, D. (2010a). Effects of diversity and procrastination in priority queuing
 522 theory: The different power law regimes. *Physical Review E - Statistical, Nonlinear, and*
 523 *Soft Matter Physics*, 81(1), 1–13. <https://doi.org/10.1103/PhysRevE.81.016108>
- 524 Saichev, A., & Sornette, D. (2010b). Generation-by-generation dissection of the response
 525 function in long memory epidemic processes. *The European Physical Journal B*, 75(3),
 526 343–355. <https://doi.org/10.1140/epjb/e2010-00121-7>
- 527 Scholz, C. H. (2015). On the stress dependence of the earthquake b value. *Geophysical Research*
 528 *Letters*, 42(5), 1399–1402. <https://doi.org/10.1002/2014GL062863>
- 529 Scholz, C. H. (2019). *The Mechanics of Earthquakes and Faulting* (3rd ed.). Cambridge:
 530 Cambridge University Press. <https://doi.org/10.1017/9781316681473>
- 531 Smith, W. D. (1981). The b-value as an earthquake precursor. *Nature*, 289(5794), 136–139.
 532 <https://doi.org/10.1038/289136a0>
- 533 Sornette, A., & Sornette, D. (1989). Self-organized criticality and earthquakes. *Europhysics*
 534 *Letters*, 9(3), 197–202. <https://doi.org/10.1209/0295-5075/9/3/002>
- 535 Sornette, A., & Sornette, D. (1999). Renormalization of earthquake aftershocks. *Geophysical*
 536 *Research Letters*, 26(13), 1981–1984. <https://doi.org/10.1029/1999GL900394>
- 537 Sornette, D. (2002). Predictability of catastrophic events: Material rupture, earthquakes,
 538 turbulence, financial crashes, and human birth. *Proceedings of the National Academy of*
 539 *Sciences of the United States of America*, 99, 2522–2529.
 540 <https://doi.org/10.1073/pnas.022581999>
- 541 Sornette, D. (2006a). *Critical Phenomena in Natural Sciences - Chaos, Fractals,*
 542 *Selforganization and Disorder: Concepts and Tools* (2nd ed.). Berlin: Springer.
- 543 Sornette, D. (2006b). Endogenous versus Exogenous Origins of Crises. In S. Albeverio, V.
 544 Jentsch, & H. Kantz (Eds.), *Extreme Events in Nature and Society* (pp. 95–119).
 545 Heidelberg: Springer. https://doi.org/10.1007/3-540-28611-X_5
- 546 Sornette, D., & Helmstetter, A. (2002). Occurrence of finite-time singularities in epidemic
 547 models of rupture, earthquakes, and starquakes. *Physical Review Letters*, 89(15), 158501.
 548 <https://doi.org/10.1103/PhysRevLett.89.158501>
- 549 Sornette, D., & Helmstetter, A. (2003). Endogenous versus exogenous shocks in systems with
 550 memory. *Physica A: Statistical Mechanics and Its Applications*, 318(3–4), 577–591.

- 551 [https://doi.org/10.1016/S0378-4371\(02\)01371-7](https://doi.org/10.1016/S0378-4371(02)01371-7)
552 Sornette, D., & Ouillon, G. (2012). Dragon-kings: Mechanisms, statistical methods and empirical
553 evidence. *European Physical Journal: Special Topics*, 205(1), 1–26.
554 <https://doi.org/10.1140/epjst/e2012-01559-5>
555 Sornette, D., Deschâtres, F., Gilbert, T., & Ageon, Y. (2004). Endogenous versus exogenous
556 shocks in complex networks: An empirical test using book sale rankings. *Physical Review*
557 *Letters*, 93(22), 1–4. <https://doi.org/10.1103/PhysRevLett.93.228701>
558 Taleb, N. N. (2010). *The Black Swan: The Impact of the Highly Improbable* (2nd ed.). London:
559 Penguin.
560 Turcotte, D. L. (1999). Self-organized criticality. *Reports on Progress in Physics*, 62(10), 1377–
561 1429. <https://doi.org/10.1088/0034-4885/62/10/201>

Geophysical Research Letters

Supporting Information for

Endo-exo framework for a unifying classification of episodic landslide movements

Qinghua Lei¹, Didier Sornette²

¹Department of Earth Sciences, Uppsala University, Uppsala, Sweden

²Institute of Risk Analysis, Prediction and Management, Academy for Advanced Interdisciplinary Studies, Southern University of Science and Technology, Shenzhen, China

Contents of this file

Text S1 to S2
Figures S1 to S16

Introduction

This document provides supporting information to complement the theory, analysis, results, and discussions in the main Letter. Text S1 describes the method for calculating normalized slope velocities. Text S2 elaborates the method of least squares for power-law calibrations. Figure S1 gives the time series of slope displacements and daily/cumulative rainfall amounts. Figures S2-S5 show the power-law calibration to the velocity data of individual extensometers around different types of peaks. Figures S6-S10 show the time series of daily slope velocities recorded by five extensometers with the peaks and troughs identified based on different detection criteria. Figure S11 shows the histogram of determined slope residual velocities. Figures S12-S14 show the histogram of power law exponents for post-peak velocity relaxation and ensemble averaged relaxation of exogenous-subcritical and exogenous-critical peaks, with peaks selected based on different criteria of time window size, relative magnitude, and coefficient of determination of the fitting. Figure S15 shows the time series of slope velocity and rainfall intensity when the slope approaches a catastrophic failure as well as the variation of normalized velocity as a function of time to the failure. Figure S16 shows the temporal variation of the shape parameter of the inverse gamma distribution of daily velocities of the Preonzo landslide as it transitions from the subcritical/critical regime to the supercritical regime.

Text S1. Calculation of normalized velocities around a peak.

We compute normalized slope velocities $\tilde{v}(t)$ around a peak based on the following equation:

$$\tilde{v}(t) = (v(t) - v_0)/(v(t_c) - v_0) \quad (\text{S1})$$

where the slope velocity $v(t)$ reaches a peak value of $v(t_c)$ at time $t = t_c$ and v_0 is the residual velocity when the landslide system has fully recovered from external perturbations. However, the determination of this residual velocity for a rainfall-induced landslide (like the Preonzo landslide) is subject to significant uncertainties, because the landslide has very rare opportunities to completely recover from one rainfall event before the next one occurs. In this work, we estimate the residual velocity by first detecting troughs in the velocity time series (see Text S2). We qualify a trough in the velocity time series as a local minimum over a 20-day time window which is at least $k = 2.5$ times smaller than the 2-month average velocity. The time window sizes and the threshold value k are chosen to give an effective and reasonable detection of peaks and troughs from the data (see Figure S2), but the results do not significantly change by varying these parameters (see Figure S7-S10 and Figure S13). We then define the residual velocity associated with a given peak as the minimum of the two nearest troughs (with one before the peak and one after the peak). Note that this residual velocity tends to vary over time reflecting the nonstationary characteristic of the landslide. Figure S11 shows the probability density function of calculated residual velocities (associated with the identified peaks in Figure 2), which have a mean of 0.008 mm/day. We have also tested other possible approaches of determining the residual velocity, e.g., based on the average of the 10 nearest troughs around a peak or based on the minimum/average of the troughs located between the former peak and the latter peak. No significant changes in the results are found.

Text S2. Power-law calibration of velocity time series around a peak.

We fit the time series of normalized velocities $\tilde{v}(t)$ around a peak to a power law:

$$\tilde{v}(t) = A/|t - t_c|^p \quad (\text{S2})$$

where t_c is the critical time chosen as the time of the peak, A is a constant, and p is the power law exponent. To estimate A and p , we use the method of least squares to minimize the following quantity:

$$s = \sum_{t_i} r(t_i)^2, \quad (\text{S3})$$

with

$$r(t_i) = \log \tilde{v}(t_i) - \log A + p \log |t_i - t_c|. \quad (\text{S4})$$

We then set the partial derivatives $\partial s / \partial (\log A)$ and $\partial s / \partial p$ to be both zero, leading to solve a linear system of two equations with the two unknowns A and p .

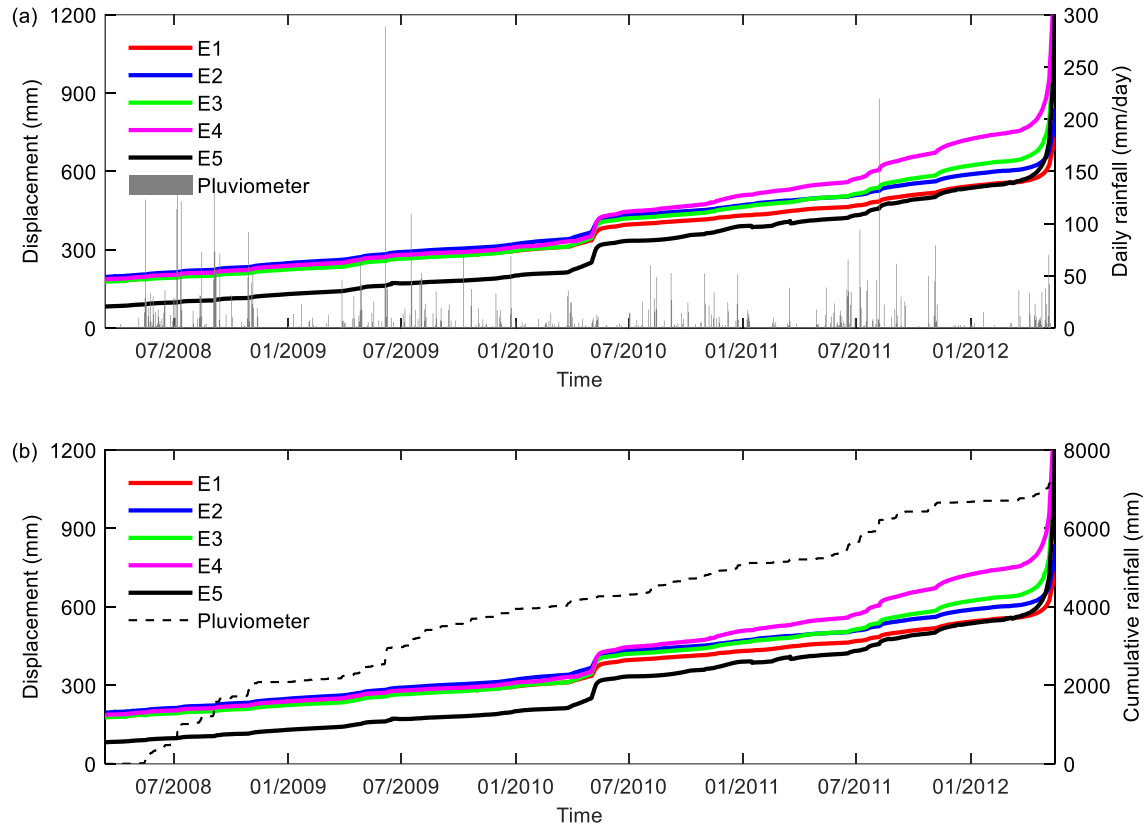


Figure S1. Monitoring data of slope displacements by the five extensometers presented together with the data of (a) daily rainfall and (b) cumulative rainfall recorded by a pluviometer installed at the Preonzo slope.

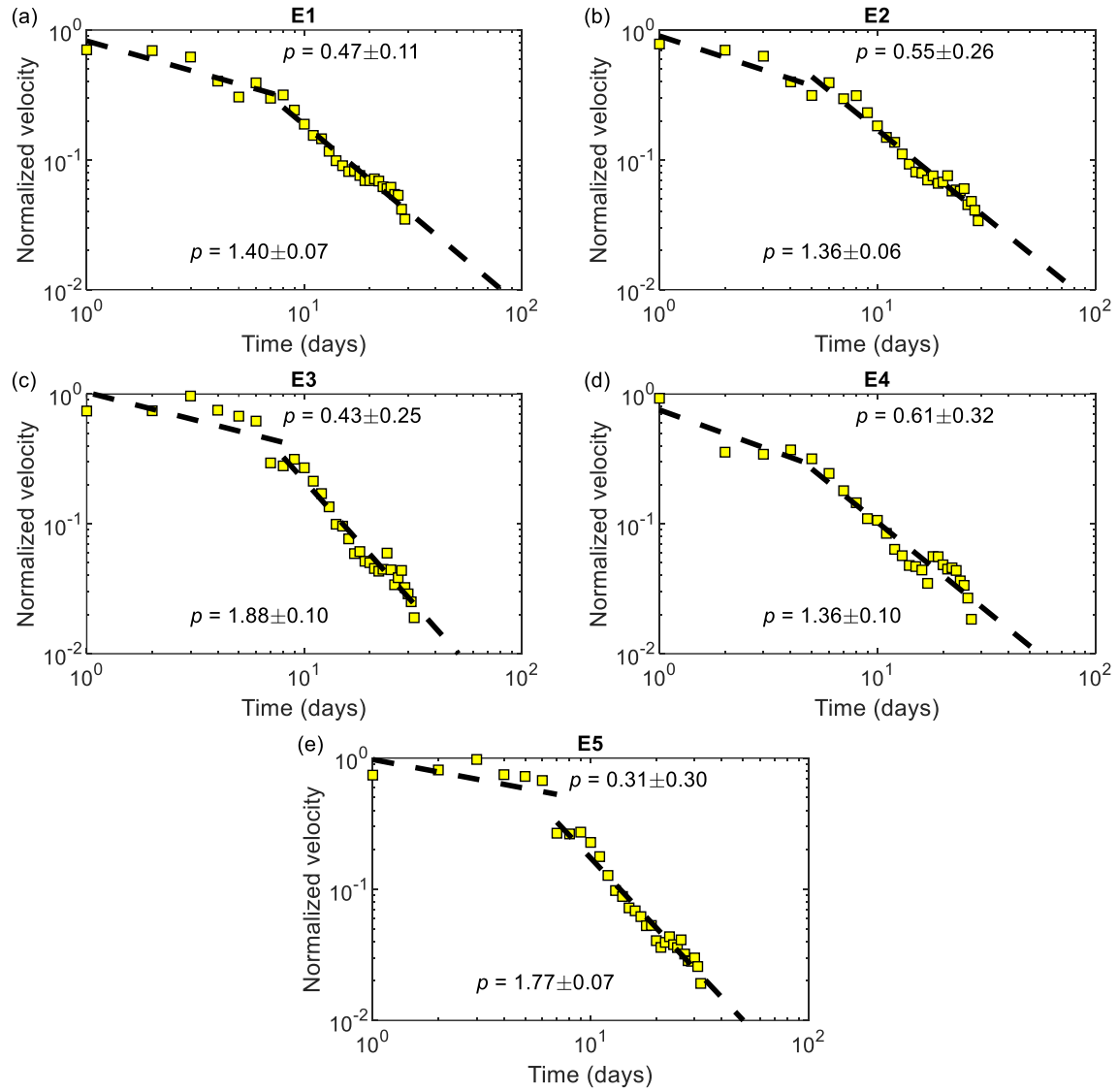


Figure S2. Post-peak relaxation of Type I exogenous-subcritical peaks based on the monitoring data of the five extensometers E1-E5.

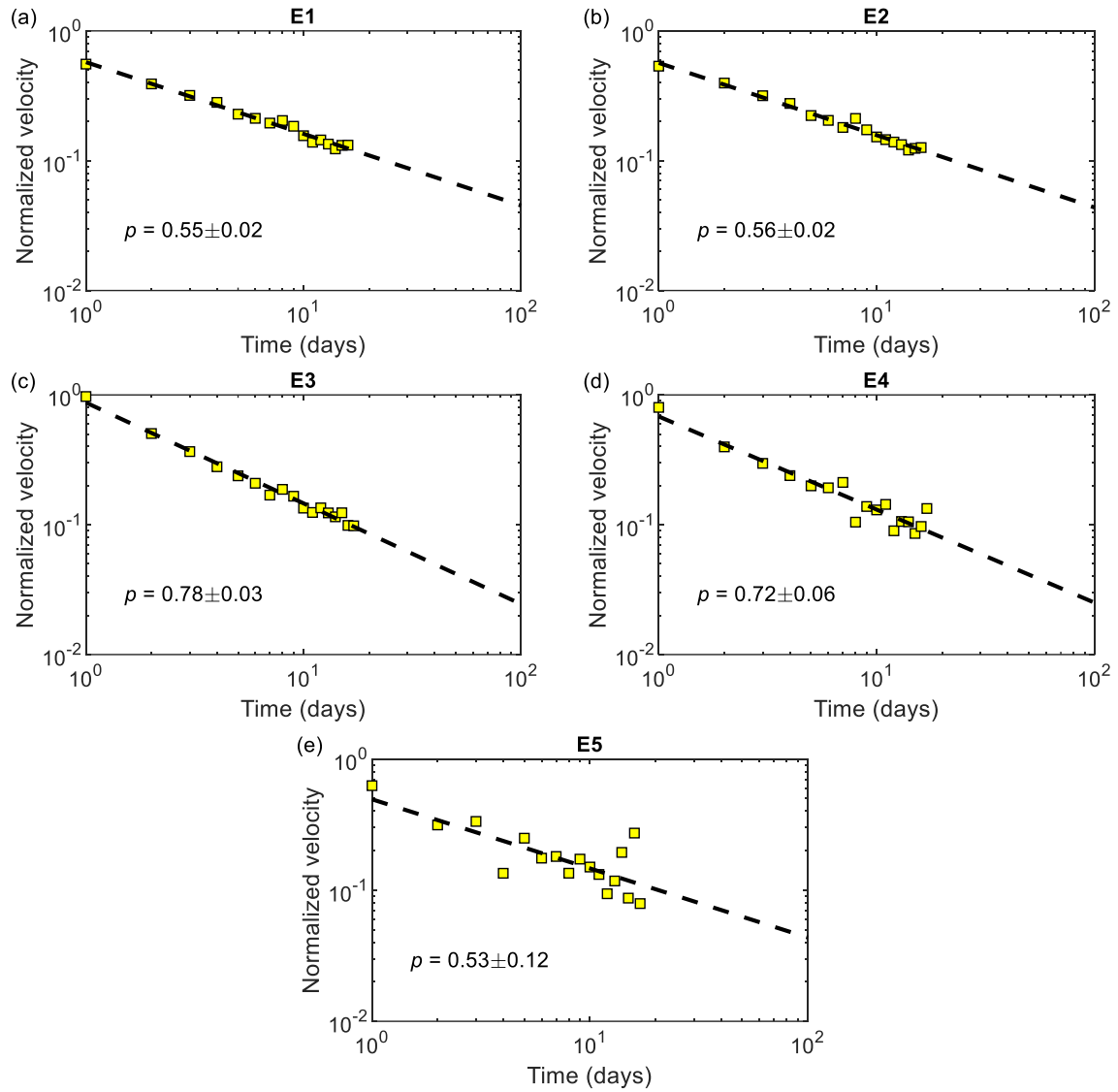


Figure S3. Post-peak relaxation of Type II exogenous-critical peaks based on the monitoring data of the five extensometers E1-E5.

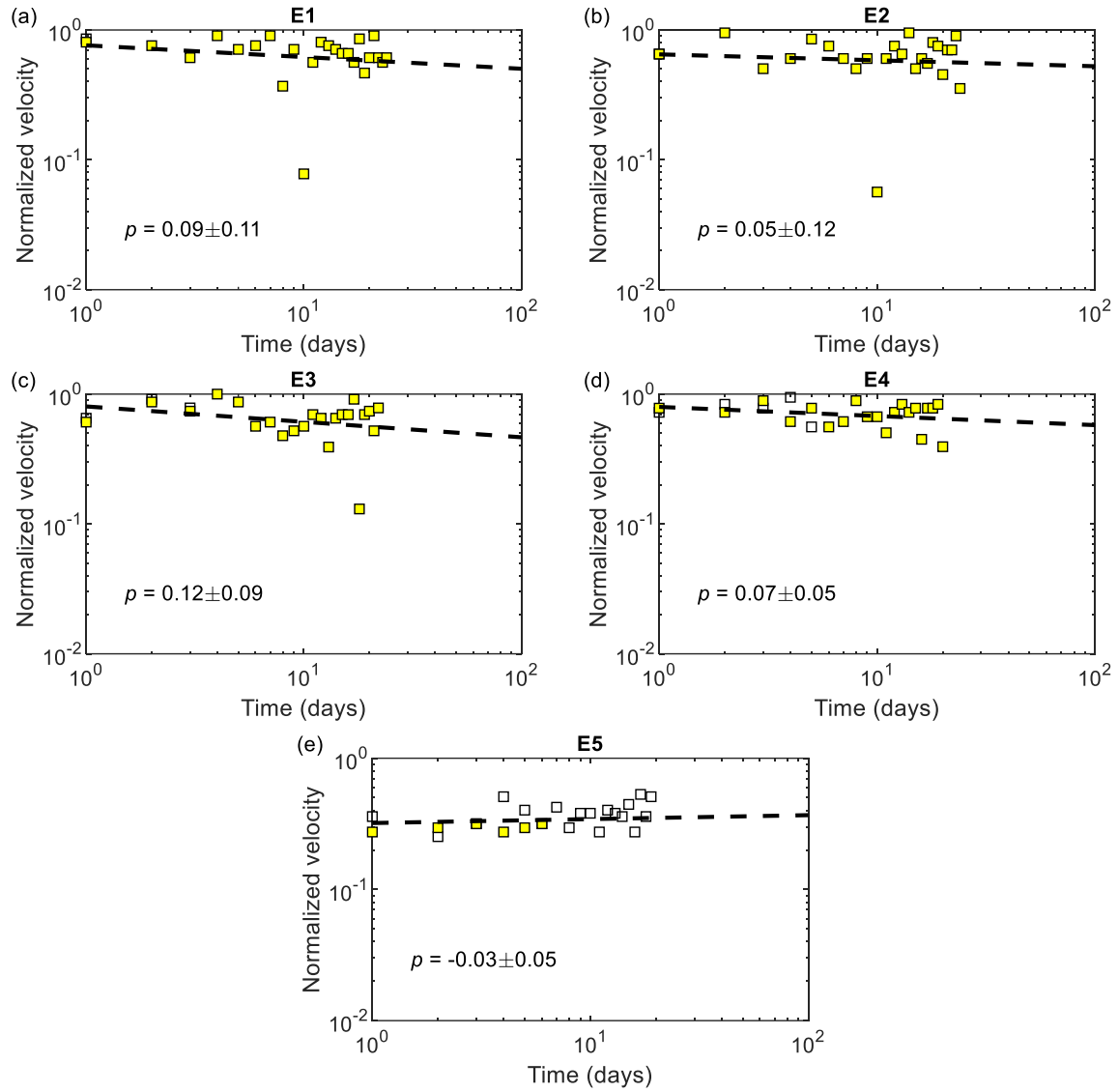


Figure S4. Pre-peak (open symbols) acceleration and post-peak (colored symbols) relaxation of Type III exogenous-subcritical peaks based on the monitoring data of the five extensometers E1-E5.

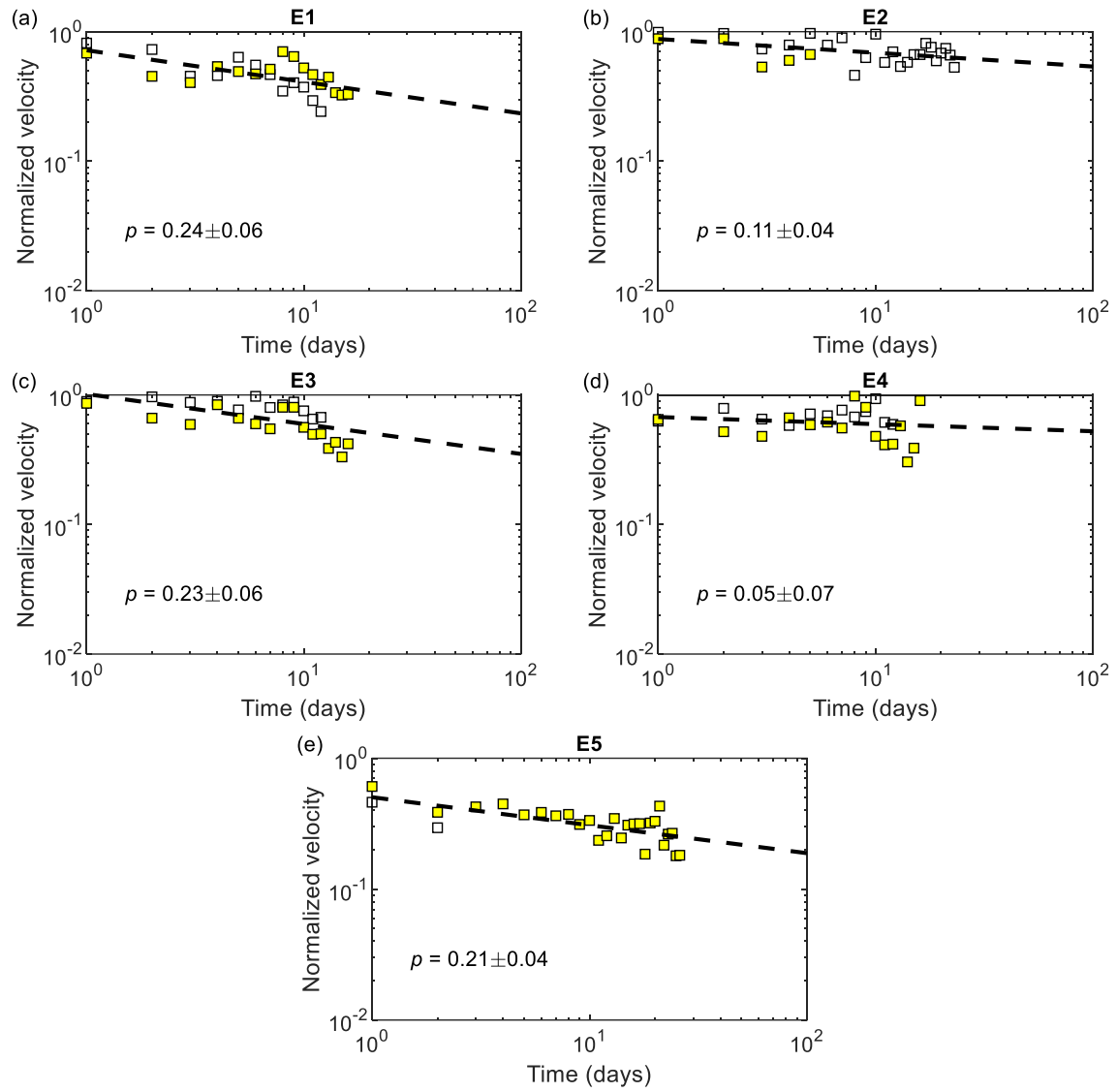


Figure S5. Pre-peak (open symbols) acceleration and post-peak (colored symbols) relaxation of Type IV exogenous-critical peaks based on the monitoring data of the five extensometers E1-E5.

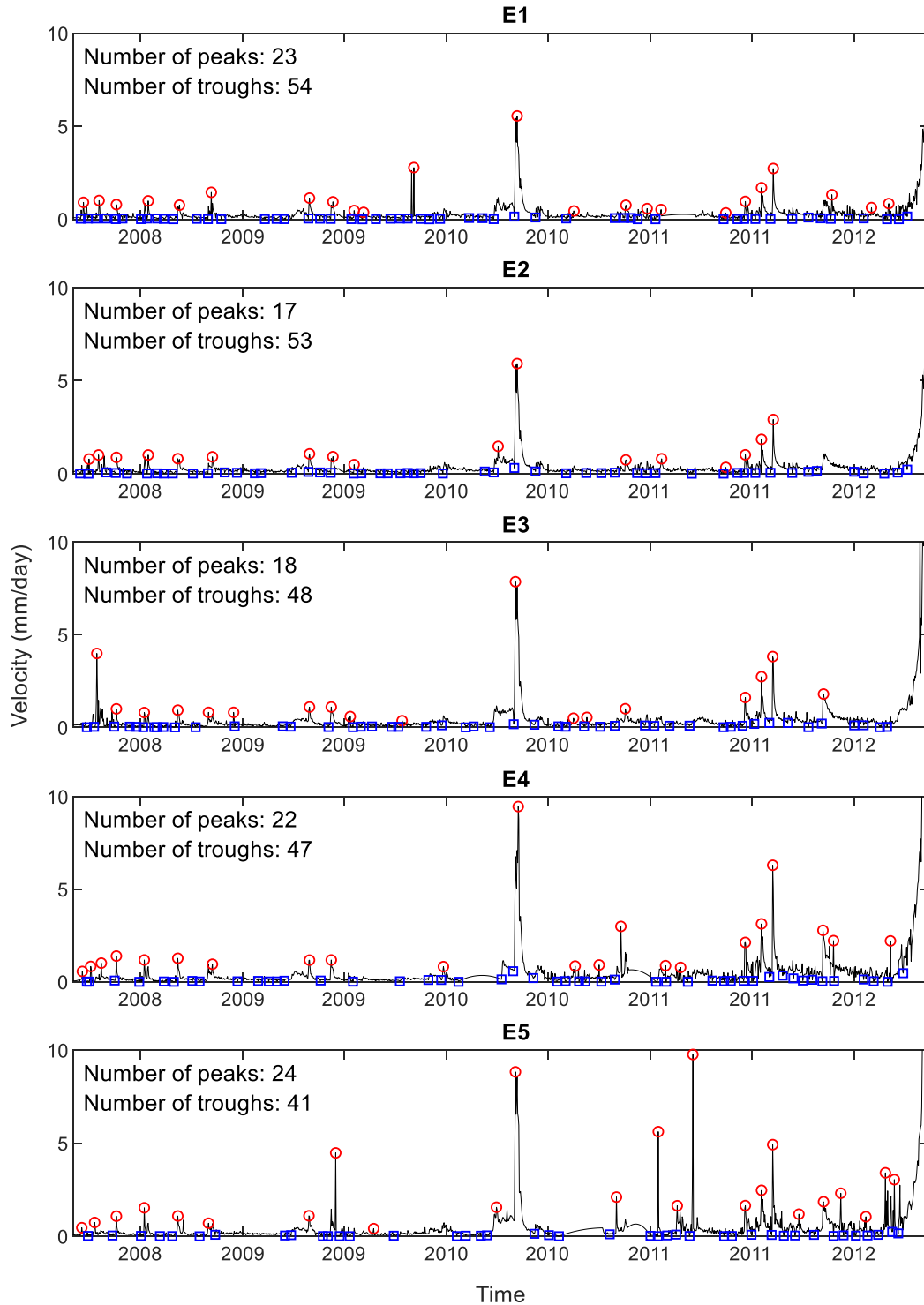


Figure S6. Time series of daily slope velocities recorded by the five extensometers E1-E5 (from top to bottom) instrumented at the Preonzo landslide, Switzerland. Peaks and troughs are marked by circles and squares, respectively. Each peak (respectively trough) is qualified as a local maximum (respectively minimum) over a 20-day time window which is at least $k = 2.5$ times larger (respectively smaller) than the average velocity over a 2-month time window.

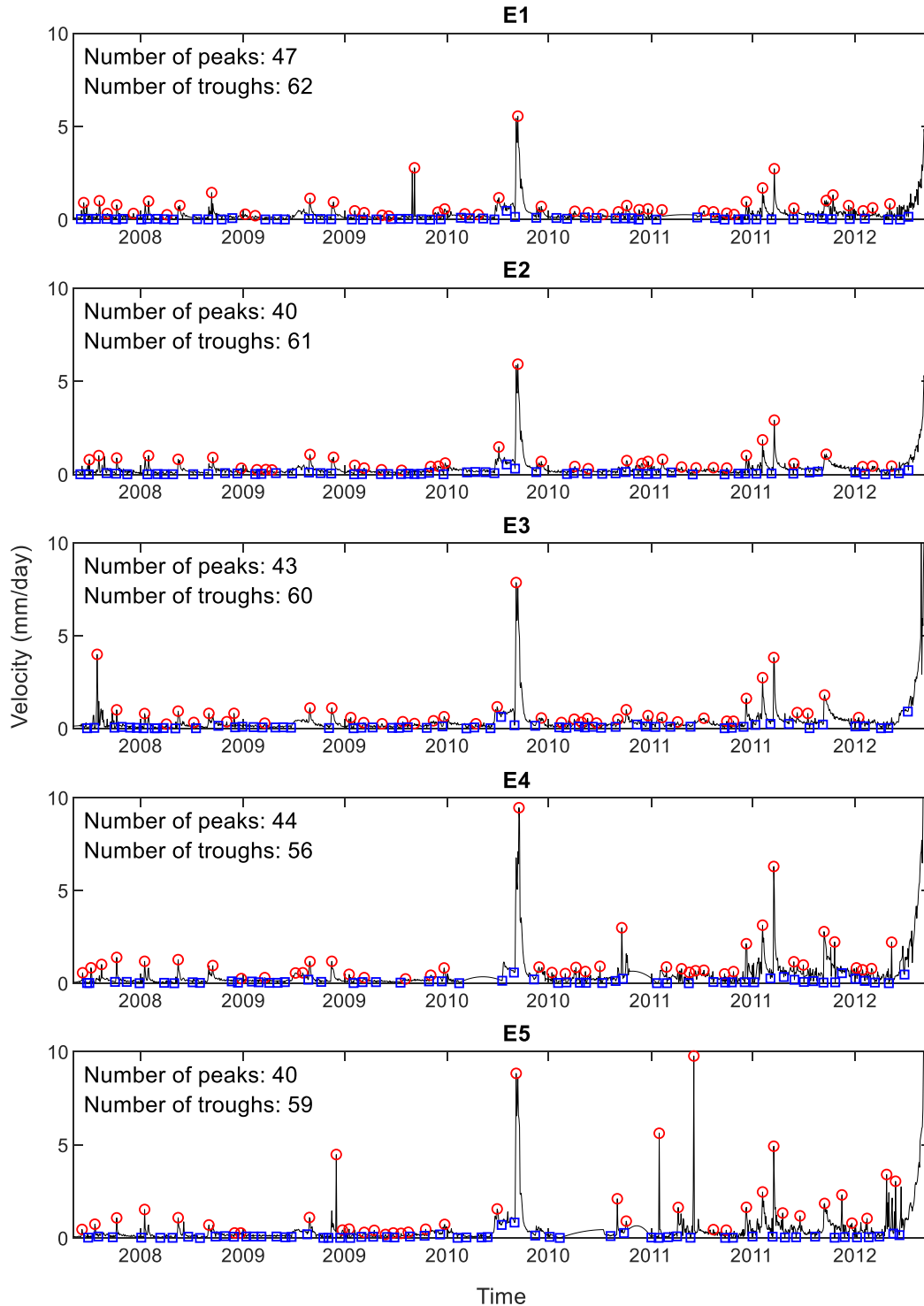


Figure S7. Time series of daily slope velocities recorded by the five extensometers E1-E5 (from top to bottom) instrumented at the Preonzo landslide, Switzerland. Peaks and troughs are marked by circles and squares, respectively. Each peak (respectively trough) is qualified as a local maximum (respectively minimum) over a 20-day time window which is at least $k = 1.5$ times larger (respectively smaller) than the average velocity over a 2-month time window.

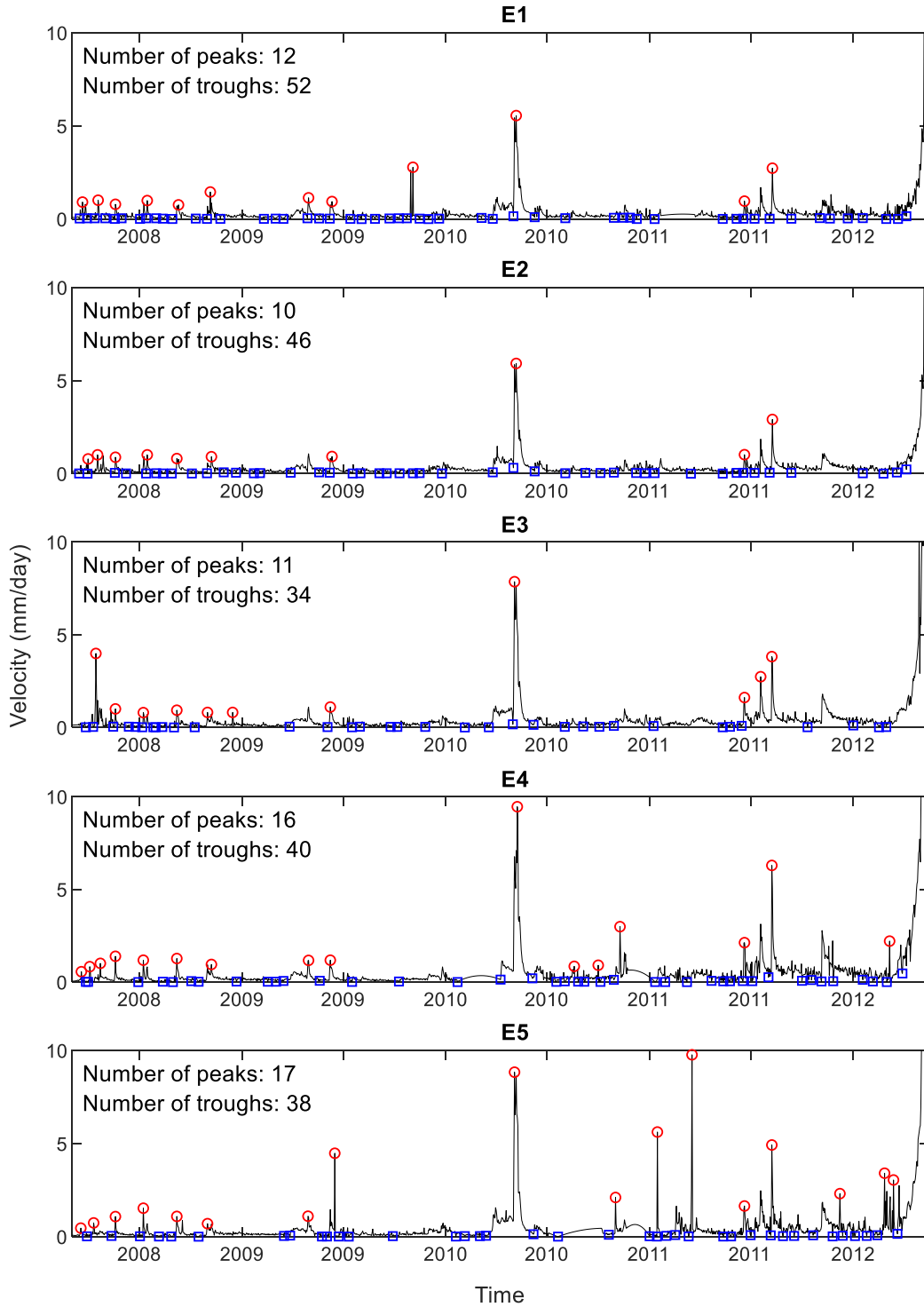


Figure S8. Time series of daily slope velocities recorded by the five extensometers E1-E5 (from top to bottom) instrumented at the Preonzo landslide, Switzerland. Peaks and troughs are marked by circles and squares, respectively. Each peak (resp. trough) is qualified as a local maximum (respectively minimum) over a 20-day time window which is at least $k = 3.5$ times larger (respectively smaller) than the average velocity over a 2-month time window.

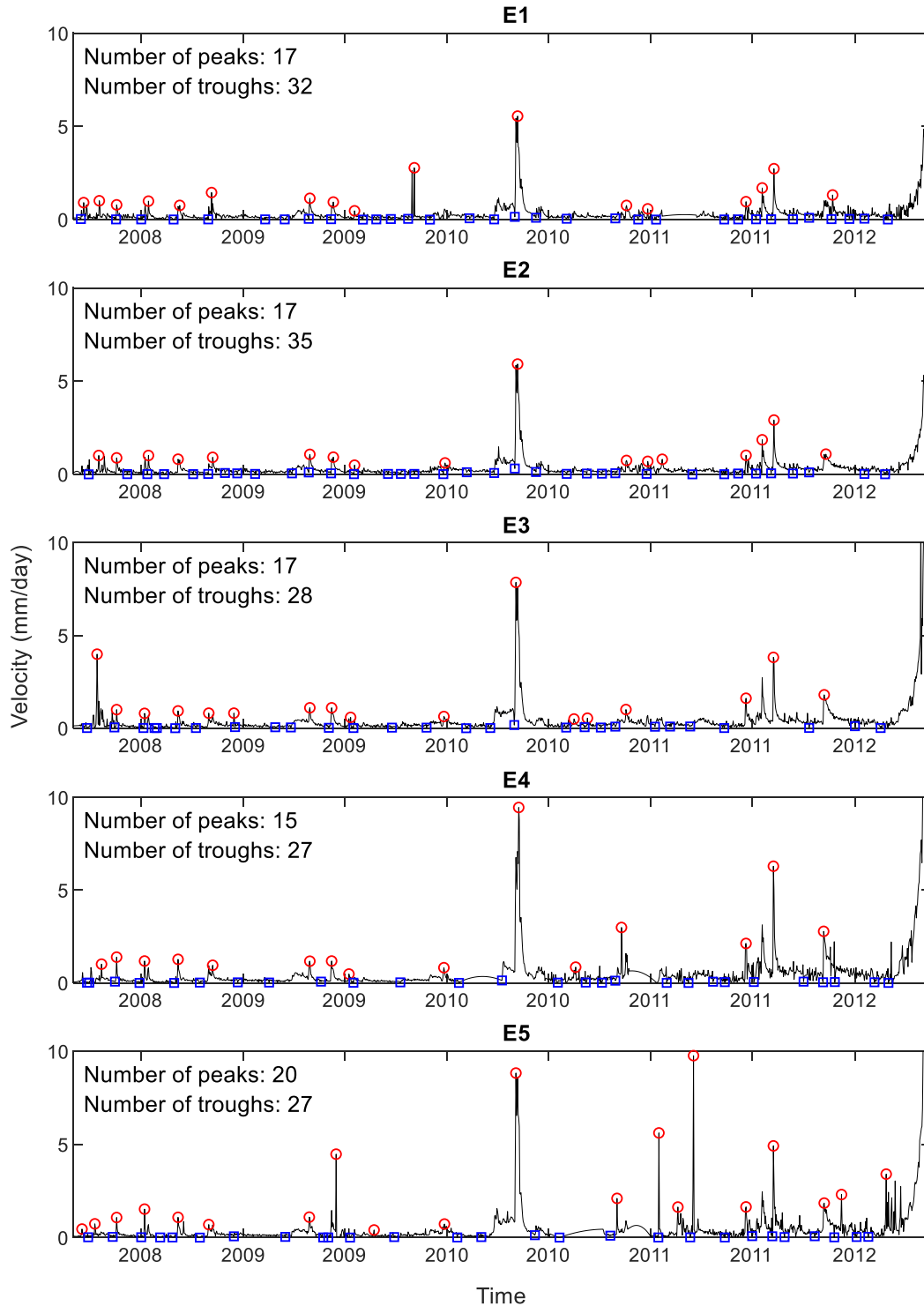


Figure S9. Time series of daily slope velocities recorded by the five extensometers E1-E5 (from top to bottom) instrumented at the Preonzo landslide, Switzerland. Peaks and troughs are marked by circles and squares, respectively. Each peak (respectively trough) is qualified as a local maximum (respectively minimum) over a 40-day time window which is at least $k = 2.5$ times larger (respectively smaller) than the average velocity over a 4-month time window.

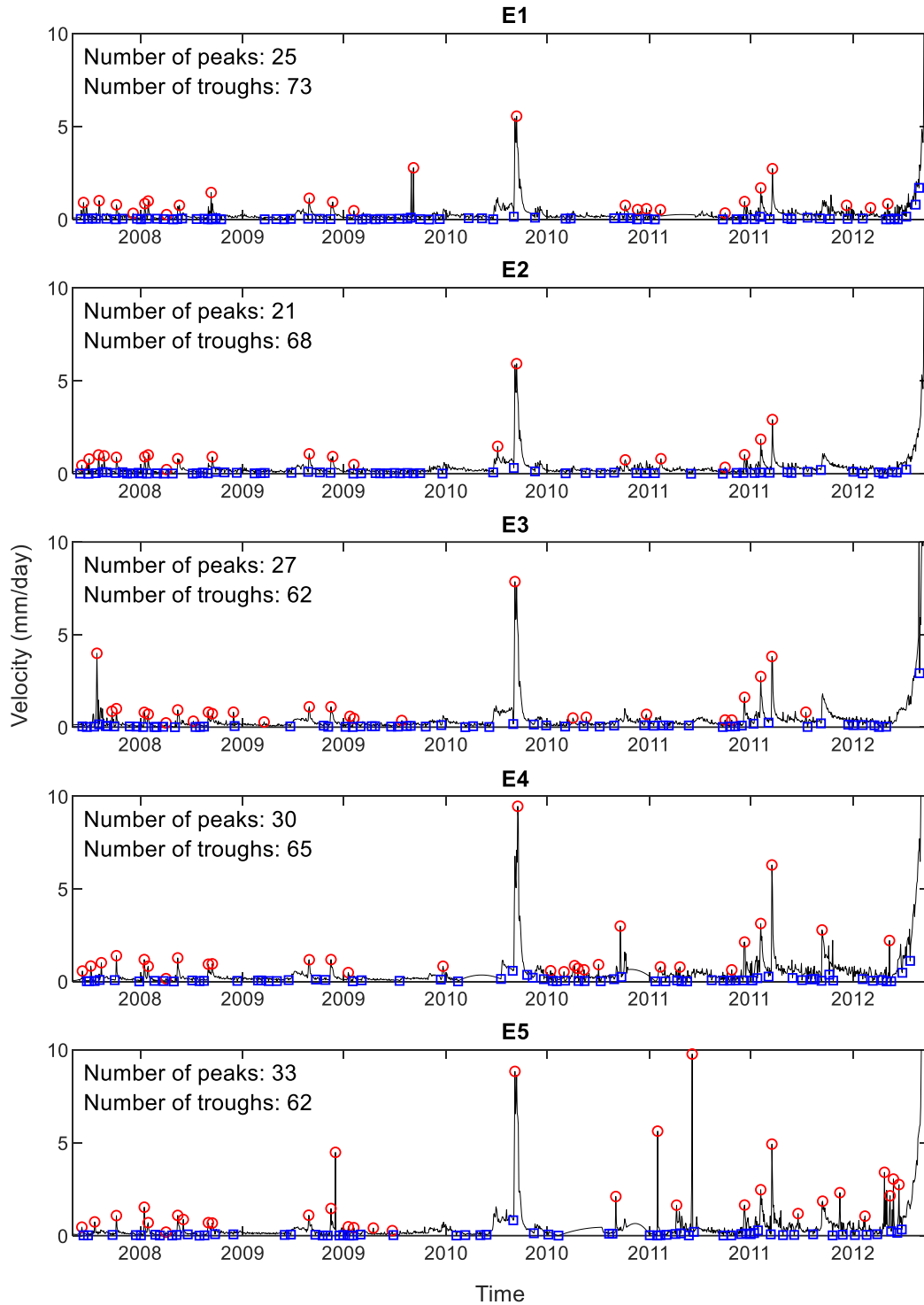


Figure S10. Time series of daily slope velocities recorded by the five extensometers E1-E5 (from top to bottom) instrumented at the Preonzo landslide, Switzerland. Peaks and troughs are marked by circles and squares, respectively. Each peak (respectively trough) is qualified as a local maximum (respectively minimum) over a 10-day time window which is at least $k = 2.5$ times larger (respectively smaller) than the average velocity over a 1-month time window.

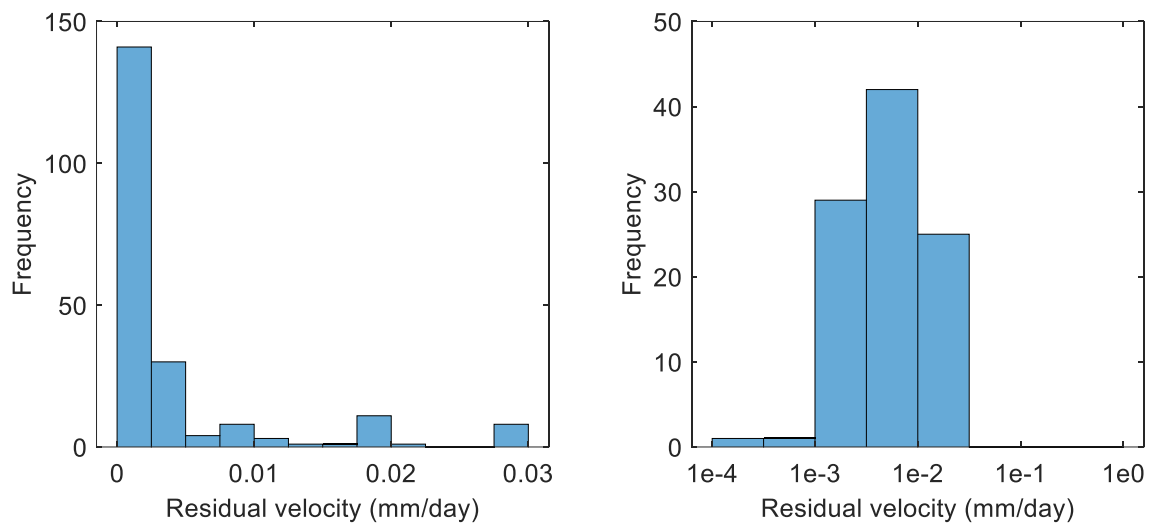


Figure S11. Histogram of slope residual velocities plotted in (a) linear scale and (b) logarithmic scale.

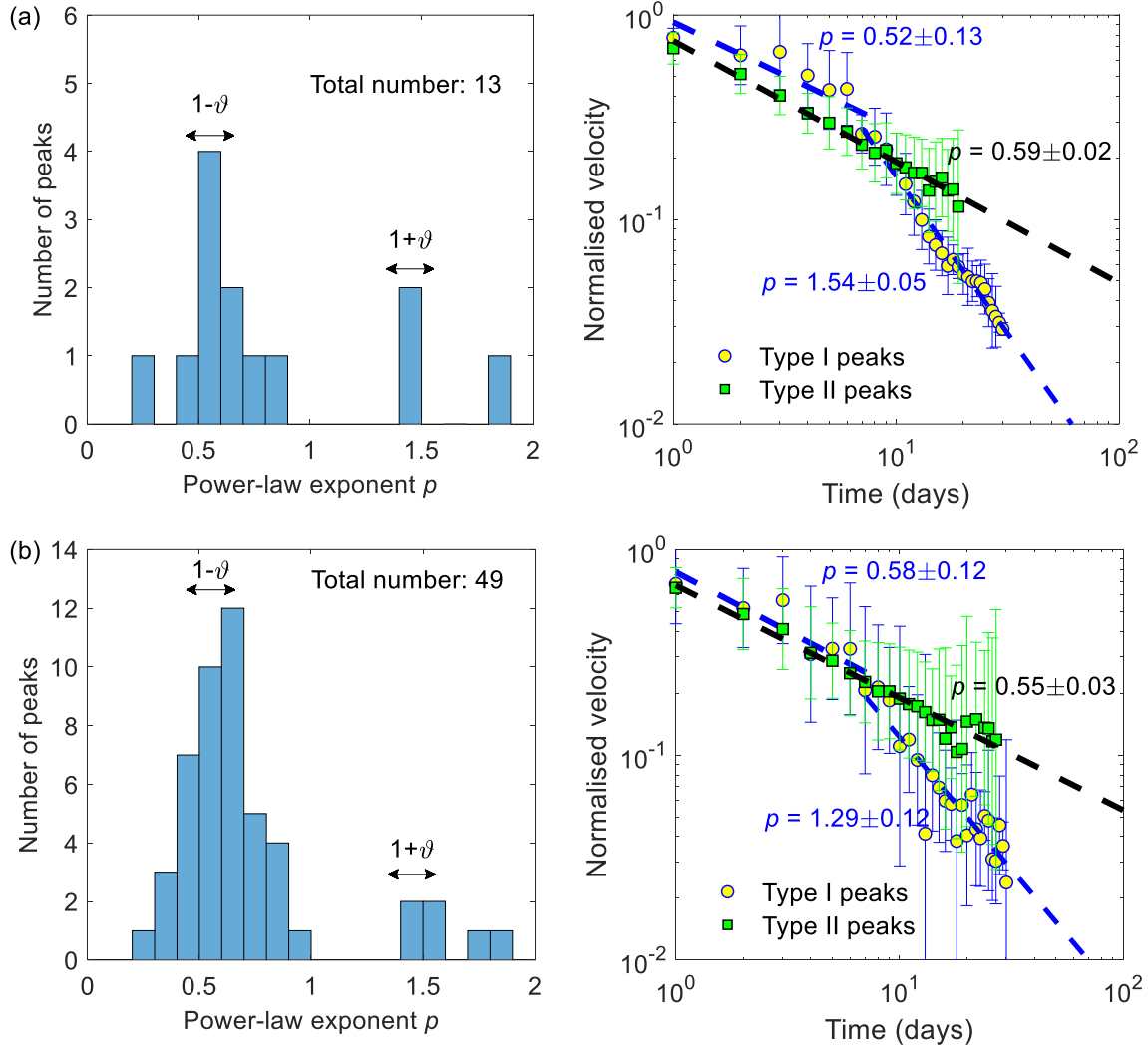


Figure S12. Left: histogram of the power law exponents p for post-peak velocity relaxation. Right: ensemble averaged relaxation of Type I (exogenous-subcritical) and Type II (exogenous-critical) peaks. Here, a peak is qualified as a local maximum over a 20-day time window which is at least $k = 2.5$ times larger than the average velocity over a 2-month time window, while the coefficient of determination for the fitting should meet (a) $R^2 > 0.9$ or (b) $R^2 > 0.7$.

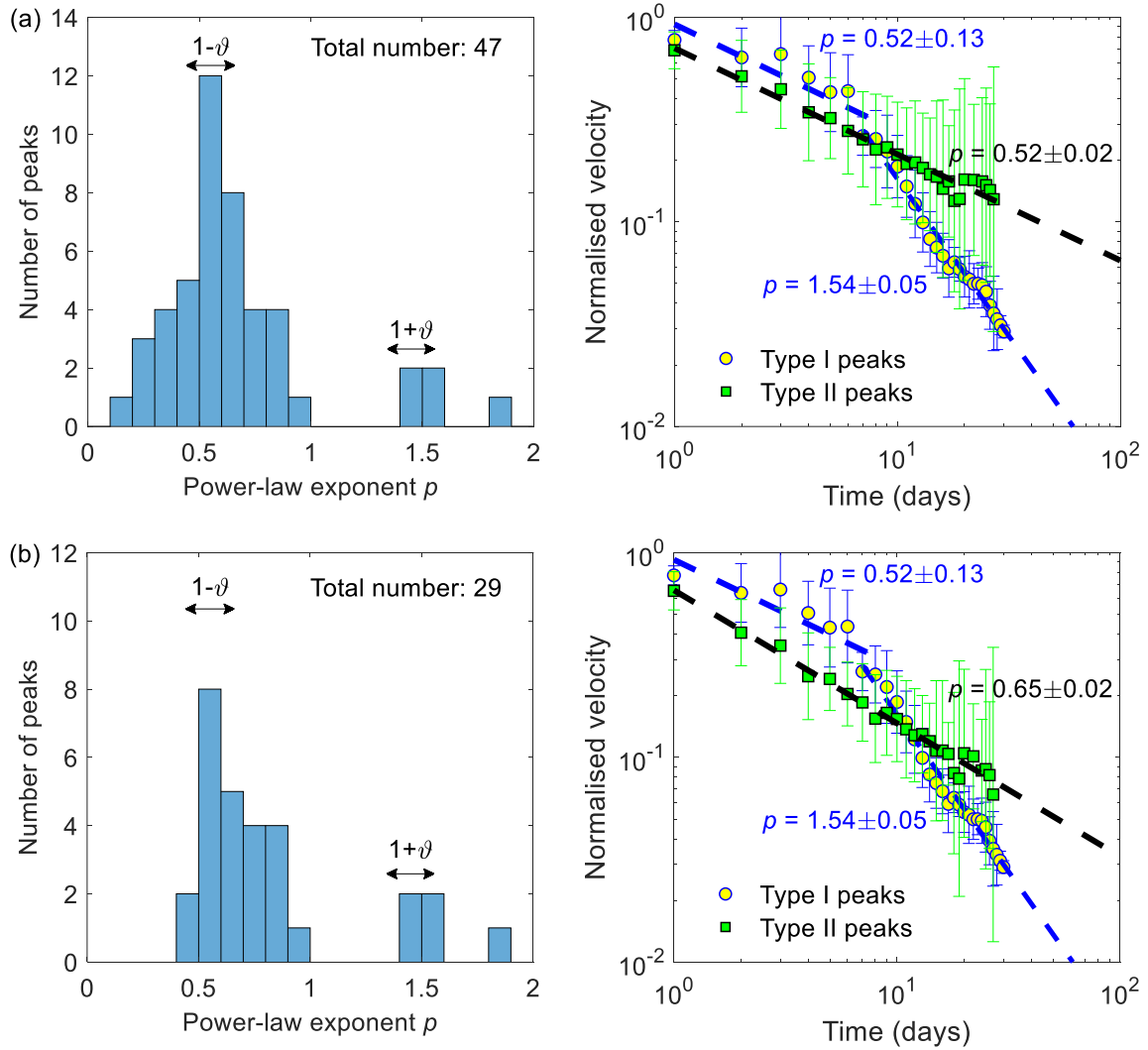


Figure S13. Left: histogram of the power law exponents p for post-peak velocity relaxation. Right: ensemble averaged relaxation of Type I (exogenous-subcritical) and Type II (exogenous-critical) peaks. Here, a peak is qualified as a local maximum over a 20-day time window which is at least (a) $k = 1.5$ or (b) $k = 3.5$ times larger than the average velocity over a 2-month time window, while the coefficient of determination for the fitting should meet $R^2 > 0.8$.

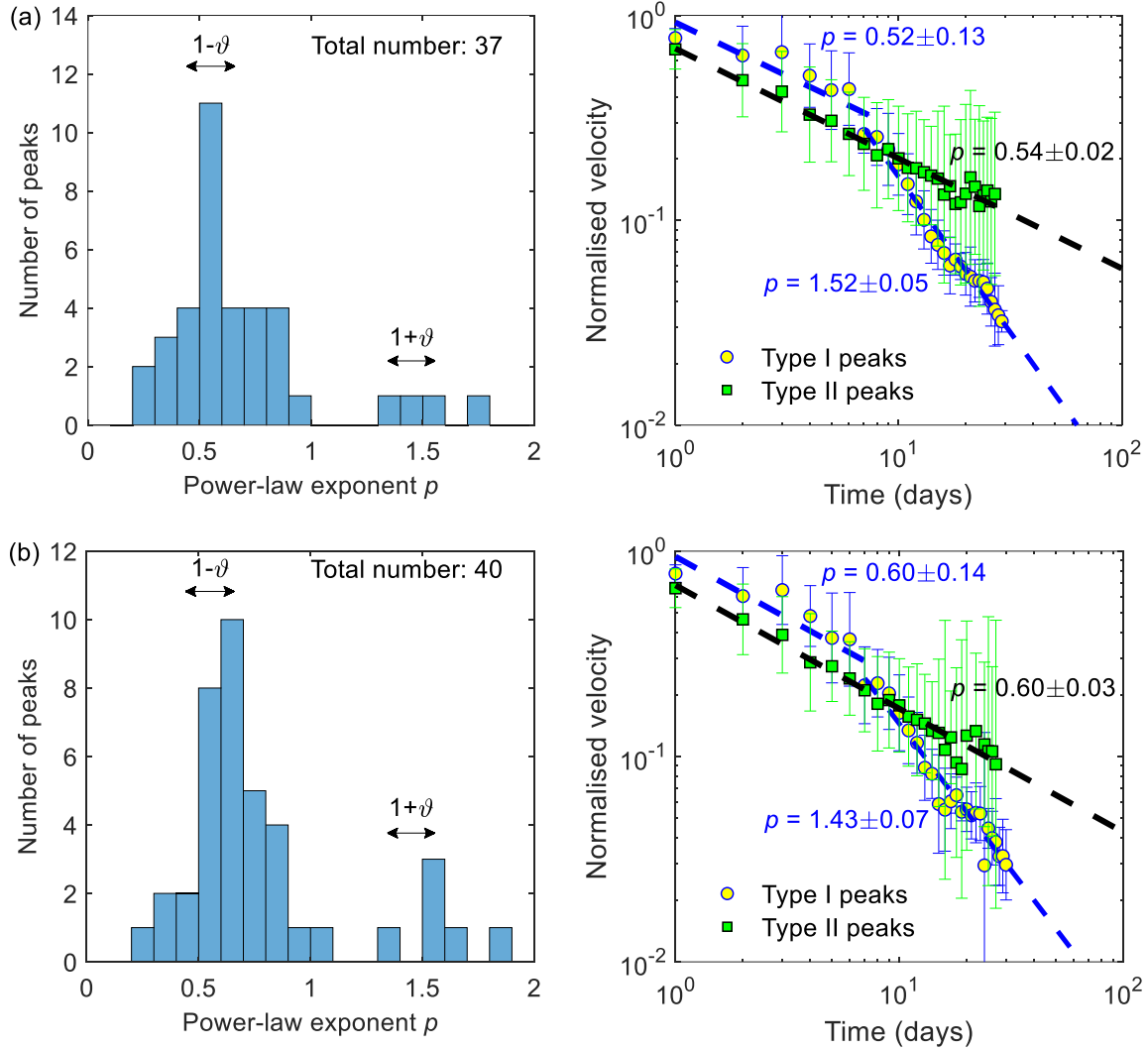


Figure S14. Left: histogram of the power law exponents p for post-peak velocity relaxation. Right: ensemble averaged relaxation of Type I (exogenous-subcritical) and Type II (exogenous-critical) peaks. Here, a peak is qualified as a local maximum over a (a) 40-day or (b) 10-day time window which is at least $k = 2.5$ times larger than the average velocity over a (a) 4-month or (b) 1-month time window, while the coefficient of determination for the fitting should meet $R^2 > 0.8$.

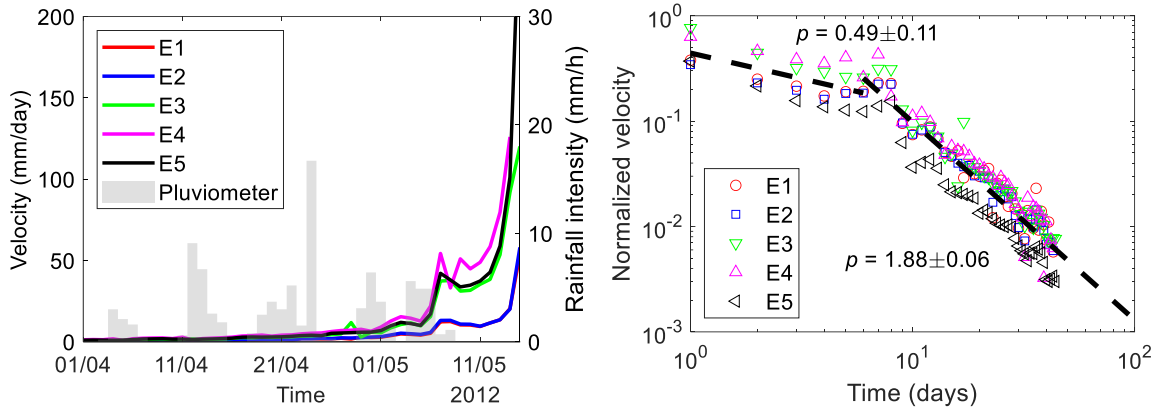


Figure S15. Left: Time series of the slope velocity measured by the five extensometers E1-E5 as well as rainfall intensity data recorded by the pluviometer for the period when the slope approaches a catastrophic failure on 15 May 2012. Right: variation of normalized velocity prior to the catastrophic failure as a function of time to the failure, which is fitted to a two-branch power law (indicated by the dashed line).

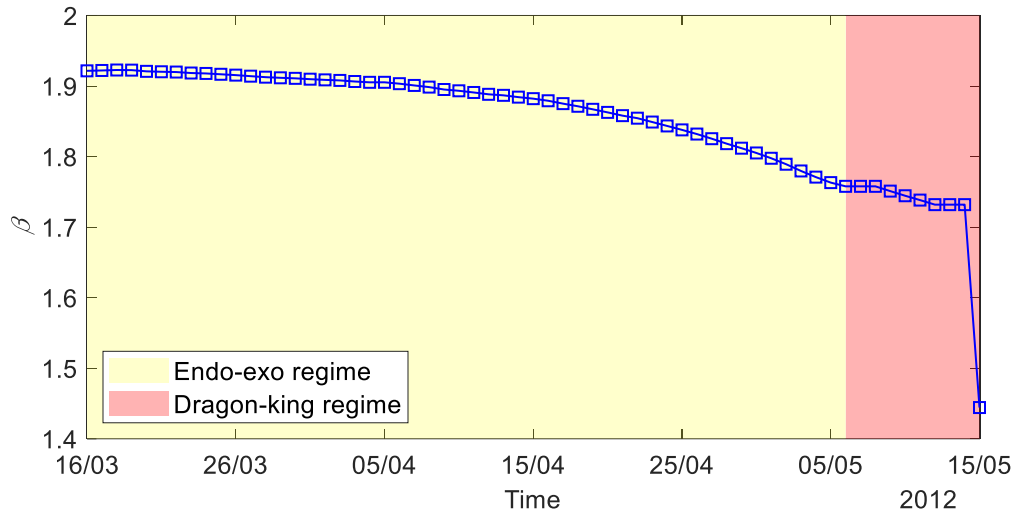


Figure S16. Temporal variation of the shape parameter β (determined based on the maximum likelihood estimation) of the inverse gamma distribution of daily velocities of the Preonzo landslide which transitions from an endo-exo (subcritical/critical) regime to a dragon-king (supercritical) regime.